Early Correction of *N*-methyl-D-aspartate Receptor Function Improves Autistic-like Social Behaviors in Adult *Shank2*$^{-/-}$ Mice

Supplementary Information

Supplementary Methods and Materials

Animals

All mice were housed and bred at the mouse facility of Korea Advanced Institute of Science and Technology (KAIST) and maintained according to the Animal Research Requirements of KAIST, except for *Shank2*$^{-/-}$ mice lacking exon 24 (corresponding to exon 15 in our nomenclature), which were bred and maintained at Duke University according to the approval of the Institutional Animal Care and Use Committee (IACUC). Mice were fed *ad libitum* under a 12-h light cycle. For every experiment performed in this research, heterozygous x heterozygous mating was used. Pups have been weaned after 21 days from birth, and 3–5 mice were grouped in each cage. The mice for behavioral assays were selected randomly and age and sex matched. All procedures were approved by the Committee of Animal Research at KAIST (KA2012_19). PCR genotyping of *Shank2*$^{-/-}$ mice lacking exons 6–7, 7, and 15 was performed using the following two sets of oligonucleotide primers: exons 6–7, set for WT allele (522 bp), forward, 5'-TGG TCT ATG TTC ATT GCA TGG-3', reverse, 5'-ATT GGC TGG GTG AGA TAC ACC-3'; set for mutant allele (626 bp), forward, 5'- CCG ACT GCA TCT GCG TGT TC-3', reverse, 5'-ATT GGC TGG GTG AGA TAC ACC-3'; exon 7, set for WT allele (698 bp) and mutant allele (299 bp), forward, 5´-TCC ATG GTT TCG GCA GAG CG-3´, reverse, 5'-CAG CAT CAT GAC AAT GTC TCC A-3´.

Drug administration

Memantine hydrochloride (Sigma, M9292; 20 mg/kg), or D-cycloserine (Sigma, C6880; 40 mg/kg), was orally administered to *Shank2*$^{-/-}$ mice twice a day with a pipette during P7–21. Memantine was also administered for a shorter period at an early stage (P7–14), for two weeks at a late stage (P25–39), or acutely at P56. To administer drugs more efficiently to mice older than P21, Nutella was coated at the end of the pipette tip. Memantine hydrochloride was dissolved in 0.1% saccharin based drinking water to reach 40 mg/ml. D-cycloserine was dissolved in 0.1% saccharin based drinking water to reach 80 mg/ml. Acute intraperitoneal injection of memantine (10 mg/kg) to mice isolated for four days was followed by a three-chamber test 30 min after the injection. These mice were subjected, after another 4-day isolation and switching of vehicle/drug treatment, to 3-chamber social interaction test, followed by an open field test the next day.

Behavioral assays

All the behavioral tests were conducted with at least 30-min habituation in the experimental rooms/booths except for the open field test, which should be a novel environment.

Three-chamber social interaction test

Three-chamber social interaction assay, a test known to measure social approach behavior [1,2], was performed as previously described [3]. Briefly, the subject mice were isolated for four days before the assay. Three-chambered apparatus consisted of left, center, and right chambers with two entrances to the center chamber. The light intensity of the apparatus was 100~130 lux. Two empty containers were located in the corner of the left or right chamber. This assay consisted of three sessions. First, the

subjects were allowed to freely explore all three chambers with empty containers in two side chambers for 10 min. Second, the subject mouse was allowed to explore the containers with a stranger mouse 1 (S1) or a novel inanimate object (O) for 10 min. Finally, the novel object was changed to a stranger mouse 2 (S2), and the subject mouse was allowed to explore the two strangers. During the interval between each session, the subject was gently guided to the center chamber and the two entrances were blocked. EthoVision XT 10 (Noldus) was used to analyze time spent in chamber or sniffing stranger/object during the first 5 min of the second and third sessions. Preference index was defined by 100 x (difference of time spent sniffing stranger mouse vs. object)/(total sniffing time).

Direct social interaction test

Direct social interactions were tested as previously described [4,5], with slight modifications. A gray test box (33 × 33 × 22 cm) with bedding under dim light (< 50 lux) was used to test direct social interaction. A juvenile male subject mouse (C57BL/6N; P28–35) with or without weaning and with or without 4-day isolation in home cages was habituated in a booth similar to the experimental booth at least for 30 min. An age- and sex-matched 129/Sv, or C3H/HeNHsd, wild-type stranger mouse was first placed in the test box and allowed to explore the box for habituation for 10 min. Next, a subject mouse was placed into the test box and allow to interact with the stranger mouse for 10 min. Direct interaction using mouse pairs under different genetic backgrounds was attempted to minimize the numbers of mice used for experiments, and was based on the previous result that inter-strain social interaction can be measured in the direct social interaction test [4]. The recorded interactions were analyzed manually by researchers blind to genotypes and experimental conditions. Social interactions were defined as activities of a WT or *Shank2*$^{-/-}$ mouse with black coat color towards a target

stranger mouse with agouti coat color, involving sniffing, following, mounting, allogrooming, huddling, and wrestling.

Olfactory test

The test procedure was slightly modified from the previous paper [6]. Briefly, we exposed mice to Kim-wipes soaked with four different odors: water, banana, coffee, stranger male mice. Pieces of Kim-wipes were placed in 60-phi Petri dishes with nine small holes in the cover. A single mouse was placed in a new home cage, and an empty petri dish was introduced for 30 min before the experiment for habituation. Each odor was sequentially presented into the cage for 4 min. This four-odor set was presented to the mouse for three times with 1-min inter-session intervals. A skilled experimenter measured the sniffing time toward Petri dishes in a blind manner.

Tube test

This assay was performed as described previously [7]. Before social dominance tests including the tube test, each mouse group (WT-V, WT-M, KO-V, and KO-M) was group housed for two weeks. We used transparent acryl tubes with 30-cm length and 3-cm inner diameter, a size that an adult mouse can just pass but usually cannot turn around. During two-day training sessions, each mouse was trained to pass through the tube in either direction for eight times. When the mice hesitated to move, they were gently pushed by a plastic bar. After the training sessions, three days of test sessions were performed. During the test sessions, animals went through three more training trials before the real test. For the test, two different mice were placed into the opposite ends of the test tube and released. The mouse first retreated from the tube was marked as a “loser”. Among six possible pairs between four cage-mates, two pairs were tested per day. Each mouse was ordered by its rank from 1 to 4.

Urine-marking test

The assay was performed as described previously [7]. As mentioned above for the tube test, each mouse group (WT-V, WT-M, KO-V, and KO-M) was co-housed for two weeks before the urine-marking test. We designed a two-chambered cage (26 cm × 21 cm × 26 cm) that are partitioned by a transparent wall with holes. A filter paper was placed at the bottom of each compartment to mark the urinated area. Two different mice in a pair were placed on the opposite sides of the wall and allowed to freely interact through the holes of the wall for 2 hours. The filter paper with marked urine was visualized under UV light, and the urine marks of each side were scored in a blind manner. The mouse with more number and larger size of urine marks was designated as a “winner”. Similar to the tube test, each mouse was ranked between 1 and 4. Urine and tube tests were performed consecutively in a random order.

Repetitive behaviors

Repetitive behaviors were measured using mice grouped in home cages. On the test day, the subject mice were allowed to freely move in a clean new cage under 100~120 lux light intensity with bedding. Amounts of time spent in digging, self-grooming, and jumping during a single 10-min session recorded were measured manually. Grooming was defined as a mouse stroking or scratching its face or body area, or licking its body. Jumping was defined as both two hind limbs simultaneously pushing against the ground. Digging was defined as a mouse uses its head or forelimbs to dig out beddings. Experiments were performed in a double-blind manner, and repetitive behaviors were manually measured.

Ultrasonic vocalization test

To perform this experiment, female young adult mice (> 8 weeks) in the same genetic

background (C57BL/6N) were used as a stranger/intruder. The subject male mice were isolated at least four days in home cages so that they recognize the cage as their own territories. A mouse in its home cage (100~120 lux) was habituated in the experimental booth for 5 min while recording basal USVs without a female intruder/stranger. Next, a female mouse was introduced into the cage, followed by recording courtship USVs of the subject mice for 5 min. Avisoft SASLab Pro software was used to analyze USVs. Spectrograms were generated with 256 Fourier transformation length, 75% overlap of temporal resolution and 45 kHz of lower cut-off frequency. USV calls longer than 2 ms were counted automatically.

Elevated plus maze test

The elevated plus maze (EPM) apparatus (center zone light intensity: 100~120 lux), located 50 cm above the ground, consisted of two open arms, two closed arms, and a neutral center zone with access to both arms. Closed arms were enclosed with 12 cm-high walls. A subject mouse was gently introduced into the center zone and allowed to move freely in the open and closed arms for 8 min. The center point of the mouse body was used to determine the entries to open/closed arms, and entry duration and frequency were measured using EthoVision XT 10.

Open field test

Open field test was performed using a 40 x 40 x 40 cm white acryl chamber (center zone light intensity: 100~120 lux). A subject mouse was gently introduced into the center zone of the chamber and recorded the movements for 1 hour. Locomotor activities and time spent in the center region of the open field arena were analyzed using EthoVision XT 10.

Laboras test

Long-term (3-day) movements of mice, including locomotor, climbing, rearing, grooming, eating, and drinking activities were recorded and automatically analyzed using the Laboratory Animal Behavior Observation Registration and Analysis System (LABORAS; Metris). Mice were individually caged in a specialized LABORAS recording environment with LABORAS cages (home-cage like) for 72 consecutive hours and fed *ad libitum*.

Electrophysiology

For hippocampal/medial prefrontal cortex (mPFC) electrophysiology experiments, sagittal/coronal sections were prepared in ice-cold dissection buffer containing (in mM) 212 Sucrose, 25 $NaHCO_3$, 10 D-glucose, 2 Na-pyruvate, 1.25 ascorbic acid, 1.25 NaH_2PO_4, 5 KCl, 3.5 $MgSO_4$, 0.5 $CaCl_2$ bubbled with 95% O_2 5% CO_2 gas. Brain sections (~300-μm thick) were prepared using Leica VT 1200 vibratome and used for whole-cell and field recordings (P13-15), 400-μm brain sections were used for juvenile (3 or 4 weeks) and adult field recording experiments. After sectioning, the slices were recovered for 30 min in normal ACSF at 32^{o}C (in mM: 124 NaCl, 25 $NaHCO_3$, 10 Glucose, 2.5 KCl, 1 NaH_2PO_4, 2 $CaCl_2$, 2 $MgSO_4$ oxygenated with 95% O_2 5% CO_2 gas). Then, the slices were moved to ACSF at room temperature and additionally recovered for 30 min. Brain slices were moved and maintained in a submerged-type recording chamber perfused with 28^{o}C ACSF (2 ml min^{-1}). Recording and stimulus glass pipettes from borosilicate glass capillaries (Harvard Apparatus) were pulled using an electrode puller (Narishige).

For extracellular recordings, the Schaffer collateral pathway in the hippocampus was stimulated every 20 sec with a pipette (0.3-0.5 MΩ) filled with

normal ACSF. Stimulation intensity was tuned to yield a half-maximal response. A recording electrode (1 MΩ) filled with normal ACSF was located in the stratum radiatum region of the hippocampal CA1 subfield to record fEPSPs, which were amplified (Multiclamp 700B, Molecular Devices) and digitized (Digidata 1550, Molecular Devices) for measurements. The averaged value of three successive rise slopes (20-50%) of fEPSP was used as a representative value of each bin (1 min). To induce LTP, stable baseline fEPSPs were maintained at least for 20 min, followed by applying high-frequency stimulation (100 Hz, 1 s). The averaged values of rise slopes for last 5 min (55 min to 60 min from LTP induction) were used for multiple comparison among experimental groups. For the input-output curve, stimulation intensity was increased every three consecutive responses; 5, 10, 15, 20, 30, 40, 50, 60, 70, 80 (in μA).

Whole-cell recordings in the CA1 region of the hippocampus and the layer 2/3 region of the medial prefrontal cortex were performed using a recording pipette (2.5-3.5 MΩ) filled with the internal solution for EPSC (in mM: 100 $CsMeSO_4$, 10 TEA-Cl, 8 NaCl, 10 HEPES, 5 QX-314-Cl, 2 Mg-ATP, 0.3 Na-GTP and 10 EGTA with pH 7.25, 295 mOsm) or IPSC (in mM: 115 CsCl, 10 TEA-Cl, 8 NaCl, 10 HEPES, 5 QX-314Cl, 2 Mg-ATP, 0.3 Na-GTP, 10 EGTA with pH 7.35, 280 mOsm). The response was amplified (Multiclamp 700B, Molecular Devices) and digitized (Digidata 1550, Molecular Devices) for measurements. Evoked EPSCs were induced by stimulating the Schaffer collateral pathway or the layer 1 of the medial prefrontal cortex with bipolar pulses (10-40 mA, 0.15 ms duration) every 15 s, while adding picrotoxin (60 μM) to ACSF to inhibit GABAergic transmission. We monitored series resistance by measuring the peak amplitude of the capacitance currents in response to hyperpolarizing step pulses (5 mV, 40 ms). Only the cells with a change in < 20% were

included in the analysis. To measure evoked AMPAR-mediated and NMDAR-mediated EPSCs, cell membrane voltages were clamped at -70 mV and +40 mV, respectively. To measure the NMDA/AMPA ratio, the average value of NMDAR currents 60 ms after the peak NMDAR currents was divided by the mean value of AMPAR current peak. We did not add an AMPAR blocker for experiments measuring the NMDA/AMPA ratio, except for those described in **Figure S22** (see the figure legend for details), because the amount of AMPAR currents remaining at 60 ms after the peak of NMDAR currents is likely to be very small [8]. In detail, 30 consecutive stable AMPAR current (above 100 pA) recordings at the holding potential of -70 mV were followed by at least 20 consecutive NMDAR current measurements at +40 mV. To calculate tau (t) constant of NMDAR currents, each NMDAR trace was fitted with exponential curve formula; $f(t) = Ae^{-t/\tau} + C$ (t is time, C is arbitrary constant, A is the amplitude of NMDAR current). For the quantification of ifenprodil effects, peak amplitudes of NMDAR currents pharmacologically isolated by NBQX (10 mM) were used for genotype comparison.

To measure paired-pulse facilitation in CA1 Schaffer collaterals and mPFC layer 2/3, paired pulses with 25, 50, 75, 100, 200, 300 ms inter-stimulus intervals were given three times and averaged, respectively.

Miniature EPSCs and IPSCs were recorded for 2 min after maintaining stable baseline for 5 min. In detail, TTX (1 μM) was added in ACSF to inhibit action potentials. For mEPSC recording, picrotoxin (60 μM) was added to ACSF. For mIPSC recording, NBQX (10 μM) and APV (50 μM) were added to ACSF to block AMPA and NMDA receptor-mediated currents.

To measure NMDAR-mediated miniature EPSCs, first whole-cell patch clamp

was done at -70 mV in normal aCSF. After 2 min stable baseline recording, ACSF with $SrCl_2$ (in mM: 124 NaCl, 25 $NaHCO_3$, 10 Glucose, 2.5 KCl, 1 NaH_2PO_4, 4 $SrCl_2$, oxygenated with 95% O_2 5% CO_2 gas) including TTX (1μM), NBQX (10μM) and picrotoxin (60μM) were applied to the slice for 8 min monitoring the baseline. After stable baseline, the mEPSCs were recorded for 2 min.

Antibodies

Antibodies against GluA1 (#1193), and GluA2 (#1195) have been previously described [9]. The following antibodies were purchased from commercial sources: Shank2 (Synaptic Systems); GluN1, PKCa (BD Transduction Laboratories); GluN2A, mGluR1, mGluR5, phospho-GluN2B (Ser 1303), phospho-GluN1 (Ser 896), GluN3A (Millipore); GluN2B (NeuroMab); CaMKIIα/β, ERK1/2, phospho-ERK1/2 (Thr 202, Tyr 204), p38, phospho-p38 (Thr 180, Tyr 182), phospho-PKA (Thr 197), phospho-PKCa (Ser 600), mTOR, phospho-mTOR (Ser 2448), phospho-GluN2B (Tyr 1472), CREB, phospho-CREB (Ser 133) (Cell Signaling); phospho-CaMKIIα/β (Thr 286), phospho-GluN2B (Ser 1480), phospho-GluN2B (Tyr 1336), PKA (Abcam), α-tubulin (Sigma).

Synaptic membrane fraction

Whole brains of *Shank2*$^{-/-}$ mice and WT littermates at postnatal day 14 and 21 were briefly homogenized in ice-cold brain homogenization buffer (0.32 M sucrose, 10 mM HEPES, pH7.4, 2 mM EDTA, 2 mM EGTA, protease inhibitors, phosphatase inhibitors). The homogenates were centrifuged at 1200 g for 10 min, and the supernatants were further centrifuged at 12000 g for 10 min. The pellet from each brain was resuspended in the brain homogenization buffer and used as a synaptic or crude membrane (P2) fraction.

In situ hybridization

Mouse brain sections (12 ㎛ thick) at embryonic day 18 (E18) and postnatal days (P0, P7, P14, P21, and P42) were prepared using a cryostat (Leica CM 1950). Hybridization probe specific for mouse Shank2 mRNA was generated using the following constructs: pGEM®T Easy vector containing nt 4608~4932 of Shank2 (NM_001113373.2). Antisense riboprobes were prepared by RNA polymerase transcription using a Riboprobe System (Promega) in the presence of a-^{35}S-UTP.

RNA-Seq library preparation and sequencing

Mouse brains were immersed in RNAlater solution (Ambion, AM7020) to stabilize RNA. RNA extraction, library preparation, cluster generation, and sequencing were performed by Macrogen Inc. (Seoul, Korea). RNA samples for sequencing were prepared using a TruSeq RNA Sample Prep Kit v2 (Illumina) according to the manufacturer's instructions. An Illumina's HiSeq 2000 were used for sequencing to generate 101-bp paired-end reads. Image analysis and base calling were performed with the standard Illumina software (RTA, Real Time Analysis v1.18). The BCL (base calls) binary was converted into FASTQ utilizing Illumina package bcl2fastq (v1.8.4).

RNA-Seq analysis

The accession series number for the RNA-Seq data is GSE82066. The raw reads were aligned to the Mus musculus genome (GRCm38) using the spliced junction mapper HISAT2 [10] (version 2.1.0, default options). The gene-level read counts were created from the aligned reads by HTSeq [11] and differential gene expression analysis was carried out using R/Bioconductor DEseq2 package (v1.19.11) [12]. The normalized read counts were computed by dividing the raw read counts by size factors and fit to a negative binomial distribution. The sequencing batch effect was adjusted between

sample groups (see GEO sample annotation) by modeling DESeq2 design formula (design = ~batch + condition). The P-values were first corrected by applying empirical estimation of the null distribution using the R fdrtool (v.1.2.15) package and then were adjusted for multiple testing with the Benjamini–Hochberg correction. Genes with an adjusted P-value less than 0.05 and with |fold-change| > 2 were considered differentially expressed.

Gene set enrichment analysis (GSEA)

The GSEA software (gsea2-2.2.4.jar) (http://software.broadinstitute.org/gsea) [13] was used to determine whether a *priori*-defined gene sets showed statistically significant differences between different groups of samples. Enrichment analysis was performed using GSEAPreranked module on gene set collections H (Hallmark gene sets; 50 gene sets), C2 (curated; 4,731 gene sets), C3 (TFT, transcription factor targets; 615 gene sets), and C5 (GO; 5917 gene sets) downloaded from Molecular Signature Database (MSigDB) v6.0 (http://software.broadinstitute.org/gsea/msigdb). GSEAPreranked is applied using the list of all expressed genes ranked by the fold change multiplied by the inverse of the p-value. At the top and bottom of the list are genes with the strongest up- and down-regulation respectively. All the recommended default settings with 1,000 permutations and a classic scoring scheme were used. The False Discovery Rate (FDR) is estimated to control the false positive finding of given Normalized Enrichment Score (NES) by comparing the tails of the observed and null distributions derived from 1000 gene set permutations. The FDR (q-value) is adjusted for gene set size but not between different comparisons. The gene sets with FDR less than 0.05 were considered significantly enriched.

Hippocampal mRNA extraction

Preparation of hippocampal mRNAs was performed using RNeasy® kit (QIAGEN).

Quantitative PCR (qPCR)

cDNAs was synthesized using TOPscript™ cDNA synthesis kit (Enzynomics, EZ005). qPCR was performed using SsoAdvanced™SYBR® Green Supermix (BIORAD,170-8882AP), CFX96™ Real-Time system, and the following primers:

Shank2 ex2-4 (1+2)	Forward	CTTCACTCAACAGGCTGGGTG
	Reverse	CTCTCCGATGCTCAGAACTTTGAC
Shank2 ex4-6 (3+4)	Forward	TGGTTCCCAGCTGAGTGTGTG
	Reverse	CCAAAGCCCTCGTTGTCCTTC
Shank2 Ex8-11 (5+6)	Forward	AGCCAGAAAGAAAGCTCCCC
	Reverse	GGCTTTGTCCACGAGTTCCT
Shank2 ex 12-13 (7+8)	Forward	TCCAAGCCCTCCAGGACTGC
	Reverse	CGAGGGAGGCCCAGAAATGG
Shank2 ex5'-8 (9+10)	Forward	GCTGTGATGATGAGCGTCCCCG
	Reverse	CTGTGGCCCACCTTGACGAC

Structural modeling

For homology-based molecular modeling of the Shank2 PDZ domain in complex with the C-terminal PDZ-binding motif (PBM) of SAPAP3, the crystal structure of the mouse Shank3 PDZ domain with the extra amino acid sequence in the immediate upstream in complex with the PBM of mouse SAPAP3 (PDB ID: 5IZU) was used as a template [14]. The homology model of the Shank2a PDZ domain (1-131 aa) was built using SWISS-MODEL modeling web server [15]. To generate the extended binding interfaces between the modeled mouse Shank2a PDZ domain and the SAPAP3 PBM, the modeled Shank2a PDZ domain was superimposed to the mouse Shank3 PDZ domain (PDB ID: 5IZU). All structural images were generated using PyMOL software [16].

Statistical analysis

Experimenters were blind to the genotype and gender of the animal tested. Before analysis, all data file names were randomized (both genotype and gender). Statistical analyses of behavioral results were performed using unpaired Student t-test or Mann-Whitney U test for the comparison of unpaired WT and KO data, paired Student t-test or Wilcoxon matched-pairs signed rank test for the comparison of paired WT and KO data, and two-way ANOVA for drug-rescue data followed by performing multiple comparisons if gene x drug interaction is significant. In non-behavioral experiments, the data from male and female mice at the juvenile or younger stage (< P28) were pooled, based on NMDAR functions (NMDA/AMPA ratio and NMDAR-dependent LTP) that are similar in males and females. Exact numbers of male and female mice used in the experiments, and details of statistical results, including main effects and p values for all possible post-hoc comparisons, are indicated in **Supplementary Table S6**.

Supplementary Figures

Supplementary fig. 1

A

P14 [KO/WT]

	Gene set name	NES	FDR p-value
C2 All	Dacosta_UV response via ERCC3 common_DN	7.026	<0.001***
	KEGG_Olfactory transduction	-6.910	<0.001***
	Reactome_Olfactory signaling pathway	-6.643	<0.001***
	Reactome_SRP dependent cotranslational protein targeting #	-6.168	<0.001***
	Reactome_Peptide chain elongation	-6.109	<0.001***
	KEGG_Ribosome	-6.067	<0.001***
	Mootha_Human MITODB_6_2002	-5.976	<0.001***
	Goldrath_Antigen response	-5.969	<0.001***
	Reactome_Influenza viral RNA transcription and replication	-5.784	<0.001***
	Gabriely_miR21 targets	5.589	<0.001***

B

P25 [KO/WT]

	Gene set name	NES	FDR p-value
C2 All	***KEGG_Ribosome***	6.703	<0.001***
	Reactome_peptide chain elongation	6.568	<0.001***
	Reactome_3_UTR_mediated translational regulation	6.164	<0.001***
	Reactome_SRP dependent cotranslational protein targeting #	6.016	<0.001***
	Reactome_Influenza viral RNA transcription and replication	5.999	<0.001***
	LEIN_Choroid Plexus markers	-5.889	<0.001***
	Reactome_Translation	5.867	<0.001***
	Reactome_Nonsense mediated decay enhanced by the exon junction complex	5.493	<0.001***
	Reactome_Influenza life cycle	5.441	<0.001***
	KEGG_Olfactory transduction	5.024	<0.001***

Figure S1. Distinct enrichment of KO(*Shank2*$^{-/-}$)/WT-P14 and KO/WT-P25 gene lists in target gene sets in the C2 category (curated gene sets).

(A and B) GSEA using two query gene lists from KO/WT-P14 and KO/WT-P25 ranked by differential expression and target gene sets in the C2 category (curated gene sets). Green and violet colors in NES indicate positive and negative enrichments, respectively; blue colors indicate target gene sets that overlap between P14 and P25. (n = 6 mice for WT and KO at P14 and P25; ***FDR < 0.001; see **Supplementary Table S3** for details).

Supplementary fig. 2

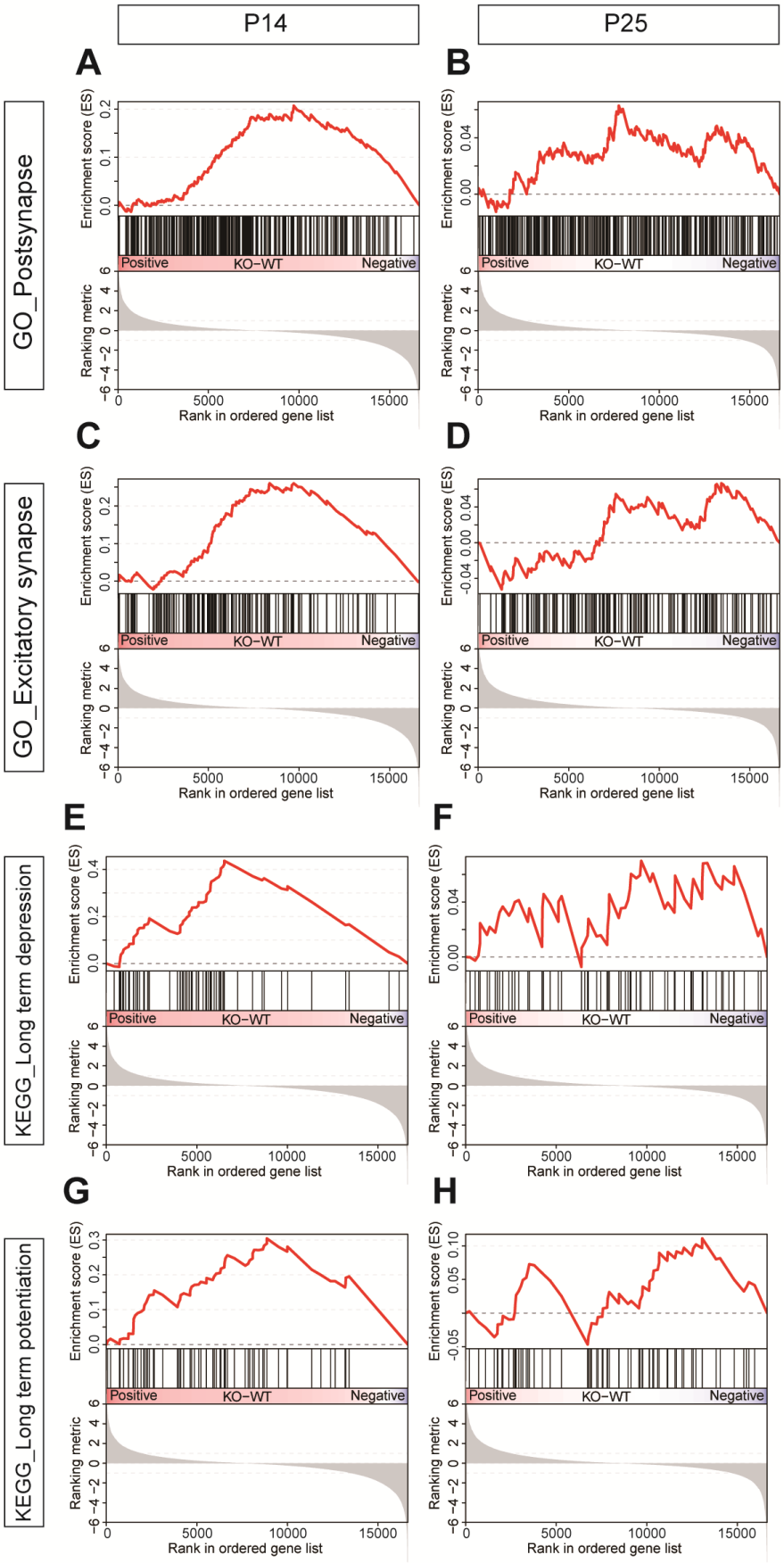

Figure S2. GSEA plots for the KO/WT-P14 and KO/WT-P25 ranked input gene lists from *Shank2*$^{-/-}$ mice and highly enriched target gene sets.

(A-H) GSEA plots for the KO/WT-P14 and KO/WT-P25 ranked input gene lists enriched for target gene sets (see Fig. 1D,E); C5CC_GO_Postsynapse (A and B), C5CC_GO_Excitatory synapse (C and D), C2_KEGG_Long term depression (E and F), and C2_KEGG_Long term potentiation (G and H). The enrichment score reflects the extent to which the genes in a target gene set falls at the top or bottom of the input gene list in this case ranked by the extent of up and down regulations. Note that the enriched genes from a particular gene set tend to fall more on the left side of the KO/WT-P14 list, relative to those more evenly distributed in the KO/WT-P25 list, leading to higher enrichment scores (n = 6 mice for P14 and P25; see **Fig. 1D,E**, and **Tables S3 and S4** for further details).

Supplementary fig. 3

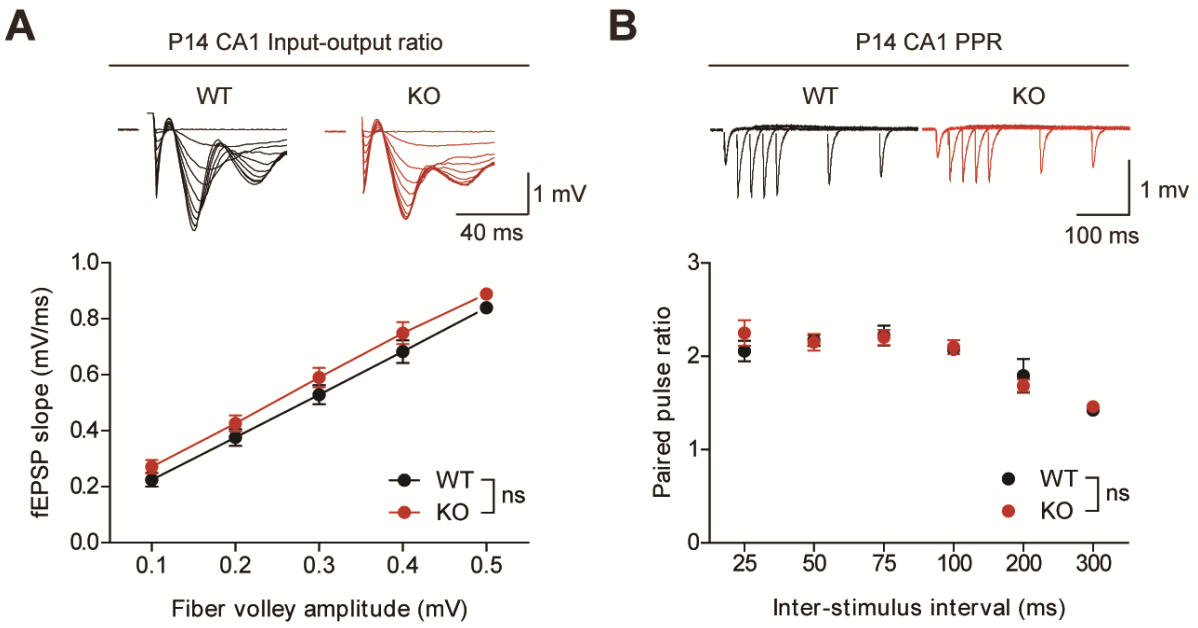

Figure S3. Normal basal synaptic transmission and paired-pulse facilitation at P14 *Shank2*$^{-/-}$ SC-CA1 synapses.

(A) Normal basal synaptic transmission at P14 *Shank2*$^{-/-}$ SC-CA1 synapses, as shown by fEPSP slopes plotted against fiber volley amplitudes. (n = 16 slices from 6 mice for WT and 19 (8) for KO at P13–15, ns, not significant, repeated measure of two-way ANOVA with Holm-Sidak test).

(B) Normal paired-pulse facilitation at P14 *Shank2*$^{-/-}$ SC-CA1 synapses, as shown by fEPSP slopes plotted against inter-stimulus intervals. (n = 9 slices from 3 mice for WT and KO at P13–15, ns, not significant, repeated measure of two-way ANOVA with Holm-Sidak test).

Supplementary fig. 4

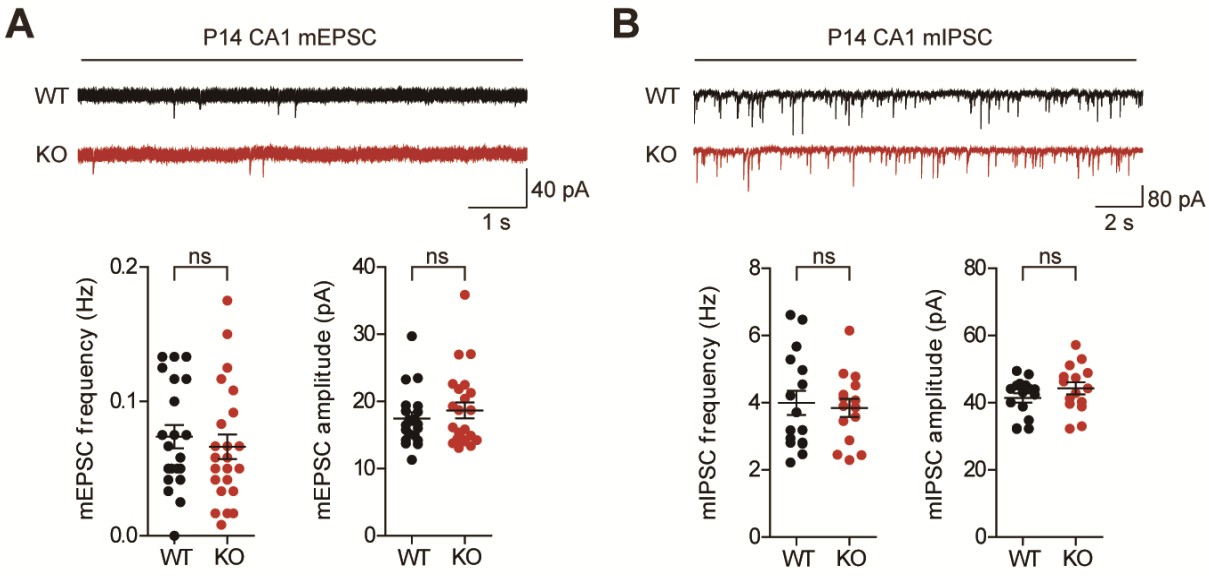

Figure S4. Normal mEPSCs and mIPSCs in P14 *Shank2*$^{-/-}$ CA1 pyramidal cells.

(A) Normal mEPSC frequency and amplitude in P14 *Shank2*$^{-/-}$ CA1 pyramidal neurons. (n = 21 neurons from 3 mice for WT and 23 (4) for KO, ns, not significant, Mann-Whitney U test).

(B) Normal mIPSC frequency and amplitude in P14 *Shank2*$^{-/-}$ CA1 pyramidal neurons. (n = 16 (3) neurons for WT and 15 (3) for KO, ns, not significant, Student t-test).

Supplementary fig. 5

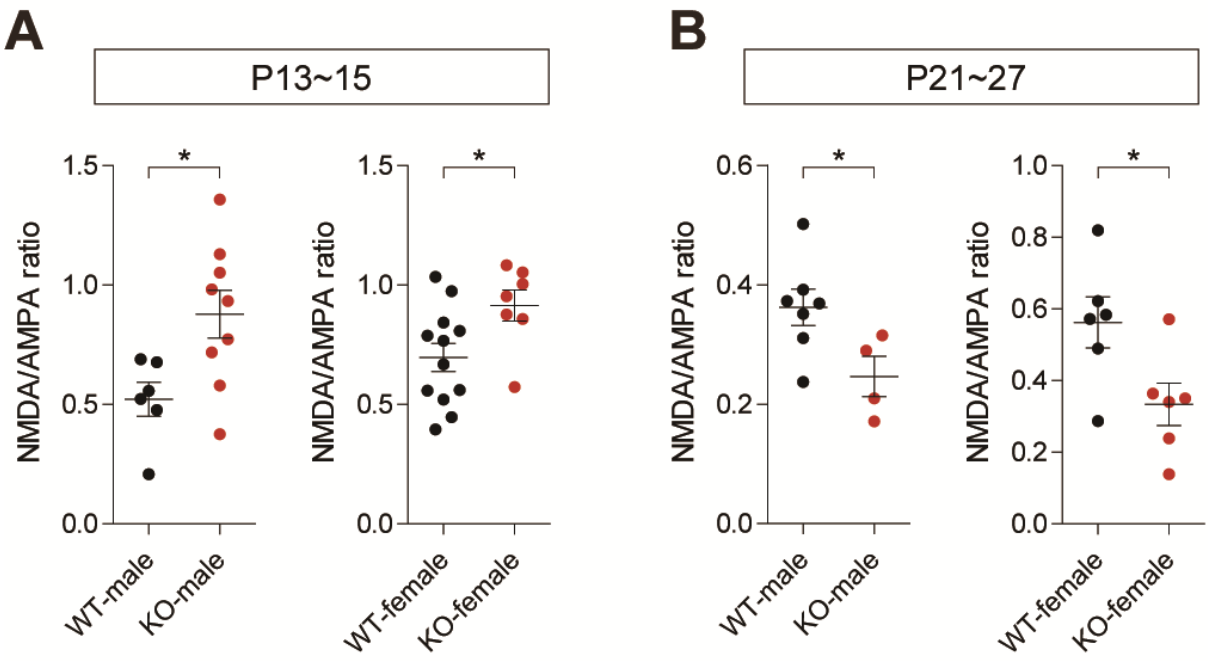

Figure S5. Gender does not affect the NMDA/AMPA ratio in *Shank2*$^{-/-}$ mice at P14 and P25.

(A and B) NMDAR function is enhanced at *Shank2*$^{-/-}$ hippocampal SC-CA1 synapses at ~P13–15, but reduced at ~P21–27 both in males or females, as shown by the NMDA/AMPA ratio. Note that the data in Fig. 2a,b were segregated into those from males and females to determine potential sexual dimorphism. (n = 6 neurons from 4 mice for WT-male and 9 (4) for KO-male, 12 (7) for WT-female, and 7 (7) for KO-female at P13–15, and 7 (5) for WT-male, 4 (2) for KO-male, 6 (3) for WT-female, and 6 (4) for KO-female at P21–27, *P < 0.05, Student t-test).

Supplementary fig. 6

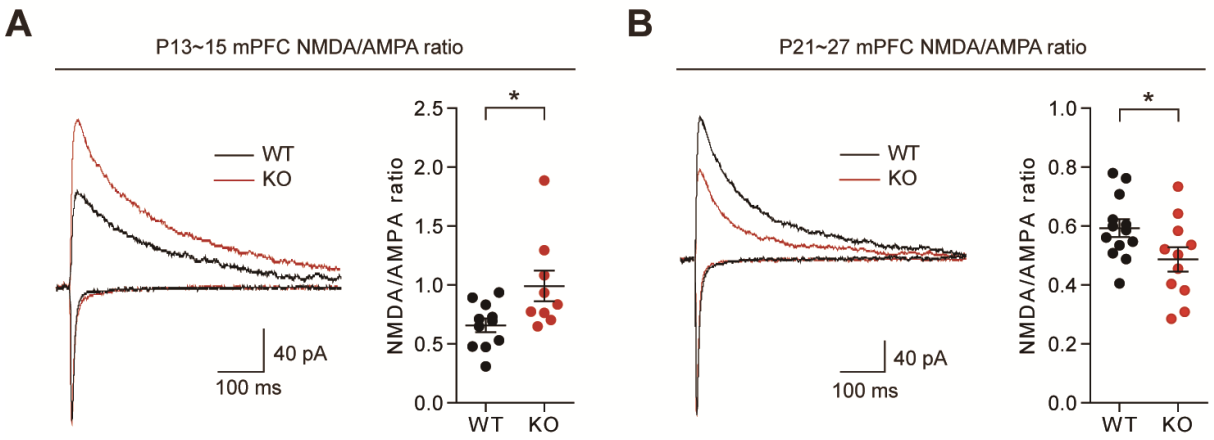

Figure S6. Enhanced and suppressed NMDAR functions in the P14 and P25 *Shank2*$^{-/-}$ mPFC.

(A and B) NMDAR function at *Shank2*$^{-/-}$ layer II/III pyramidal synapses is enhanced at ~P13–15, but reduced at ~P21–27, as shown by the NMDA/AMPA ratio. (n = 11 neurons from 4 mice for WT and 9 (4) for KO at P13–15, and 13 (6) for WT and 11 (7) for KO at P21–27, **P* < 0.05, Student t-test).

Supplementary fig. 7

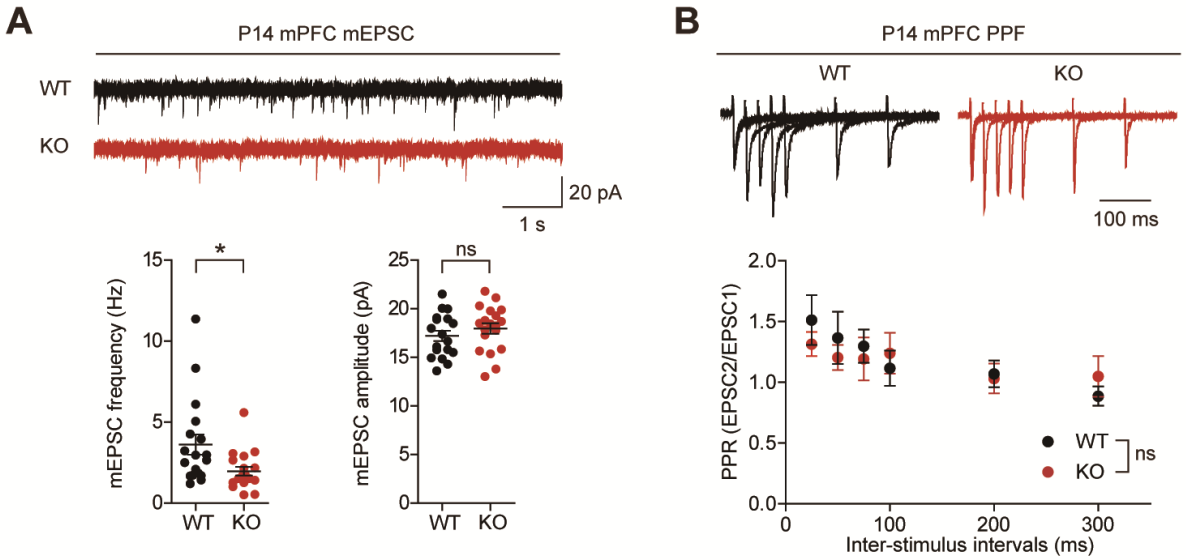

Figure S7. Normal amplitude, but reduced frequency, of mEPSCs and normal paired-pulse facilitation in the P14 *Shank2*$^{-/-}$ mPFC.

(A) mEPSC amplitude and frequency in P14 *Shank2*$^{-/-}$ mPFC layer II/III pyramidal neurons. (n = 18 neurons from 4 mice for WT and 19 (4) for KO, **P* < 0.05, ns, not significant, Mann-Whitney U test for frequency, and Student t-test for amplitude).

(B) Normal paired-pulse facilitation in P14 *Shank2*$^{-/-}$ mPFC layer II/III pyramidal neurons. (n = 7 neurons from 3 mice for WT and 5 (2) for KO, ns, not significant, repeated measures two-way ANOVA with Holm-Sidak test).

Supplementary fig. 8

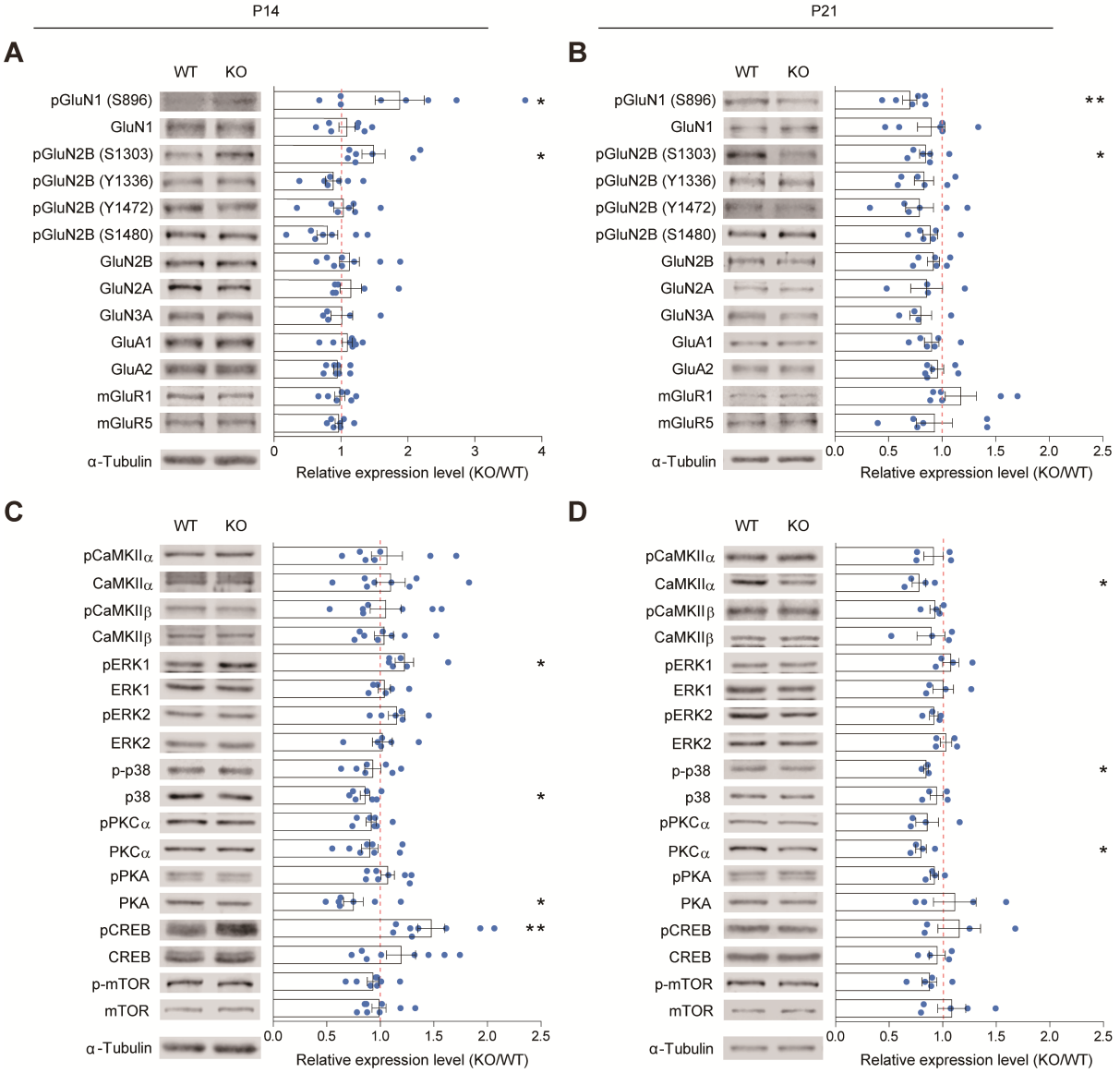

Figure S8. Total and phosphorylation levels of glutamate receptors and signaling molecules in P14 and P21 *Shank2*$^{-/-}$ brains.

(A–D) Whole-brain crude synaptosomes from P14 and P21 WT and *Shank2*$^{-/-}$ (KO) mice were immunoblotted for total and phosphorylated glutamate receptor subunits and signaling proteins. KO band/a-tubulin signals were normalized to WT/a-tubulin values. (n = 4~8 mice for WT and KO, ns, not significant, **P* < 0.05, ***P* < 0.01, one sample t-test). Note that some of the immunoblot results here, including that for GluN1, are different from our previous results [3] for reasons, including that the two experiments

used mice at different ages (we do not know the exact ages of the mice used in the previous study other than an age range [3–4 weeks]), mice of different male-female ratios (2 + 2 in the previous study vs. 2 + 4, i.e. for GluN1, in the present study), mice at different generations (genetic backgrounds might have drifted), mice bred in two very different environments (institutions in different cities), or mice sacrificed using different methods (cervical dislocation vs isoflurane).

Supplementary fig. 9

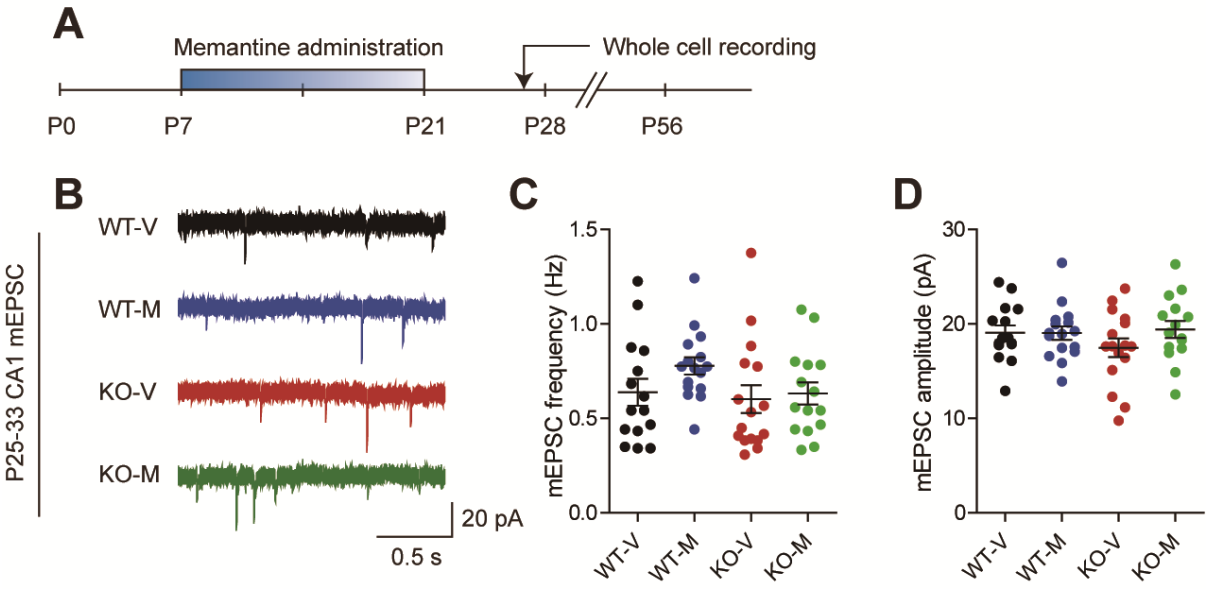

Figure S9. Early memantine treatment has no effect on mEPSCs in *Shank2*$^{-/-}$ hippocampal CA1 pyramidal neurons.

(A–D) mEPSC frequency and amplitude in the CA1 pyramidal neurons in WT and *Shank2*$^{-/-}$ mice (P26–33) treated with early memantine or vehicle (P7–21). Examples of currents traces (b). (n = 15 neurons from 4 mice for WT-V, 16 (3) for WT-M, 16 (3) for KO-V, and 15 (3) for KO-M, two-way ANOVA for (c and d)).

Supplementary fig. 10

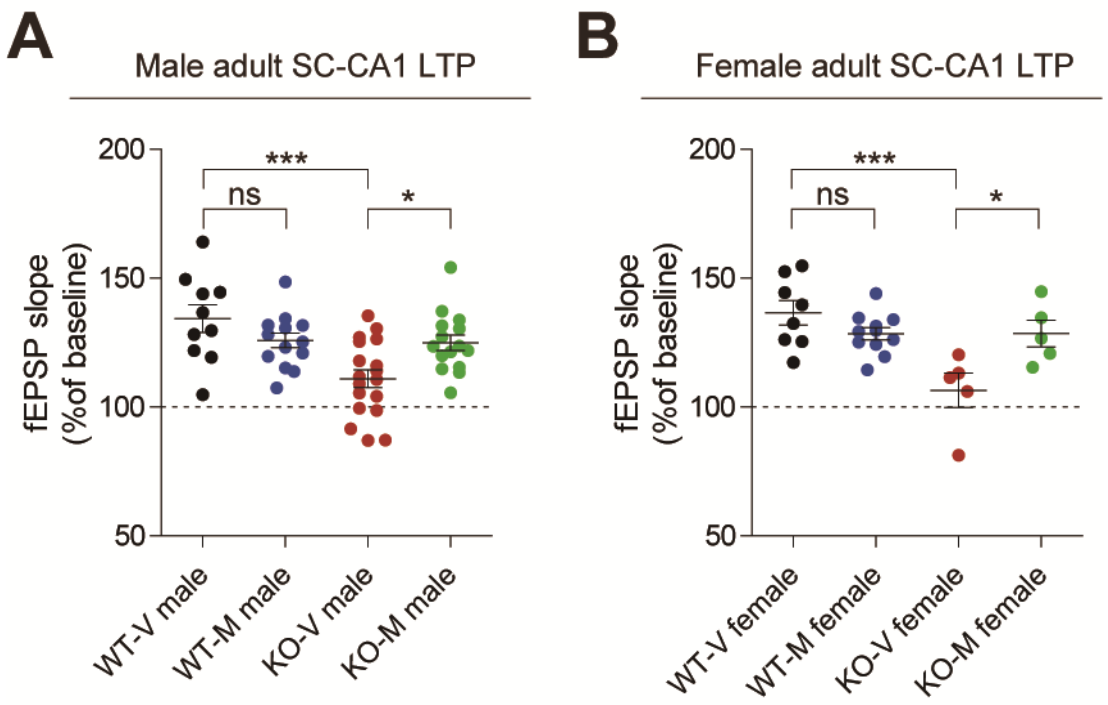

Figure S10. Gender does not affect NMDAR-dependent LTP and its memantine-dependent rescue in *Shank2*$^{-/-}$ mice.

(A and B) NMDAR-dependent LTP is suppressed at *Shank2*$^{-/-}$ SC-CA1 synapses at ~P56–84, and memantine-dependent rescues of NMDAR-dependent LTP are similar in males and females. Note that the data in **Fig. 3C** were segregated into those from males and females to determine potential sexual dimorphism. (n = 10 slices from 5 mice for WT-V, 14 (8) for WT-M, 18 (7) for KO-V and 15 (5) for KO-M in males, and 8 (4) for WT-V, 11 (4) for WT-M, 5 (2) for KO-V and 5 (2) for KO-M in females, **P* < 0.05, ****P* < 0.001, ns, not significant, two-way ANOVA with Holm-Sidak test).

Supplementary fig. 11

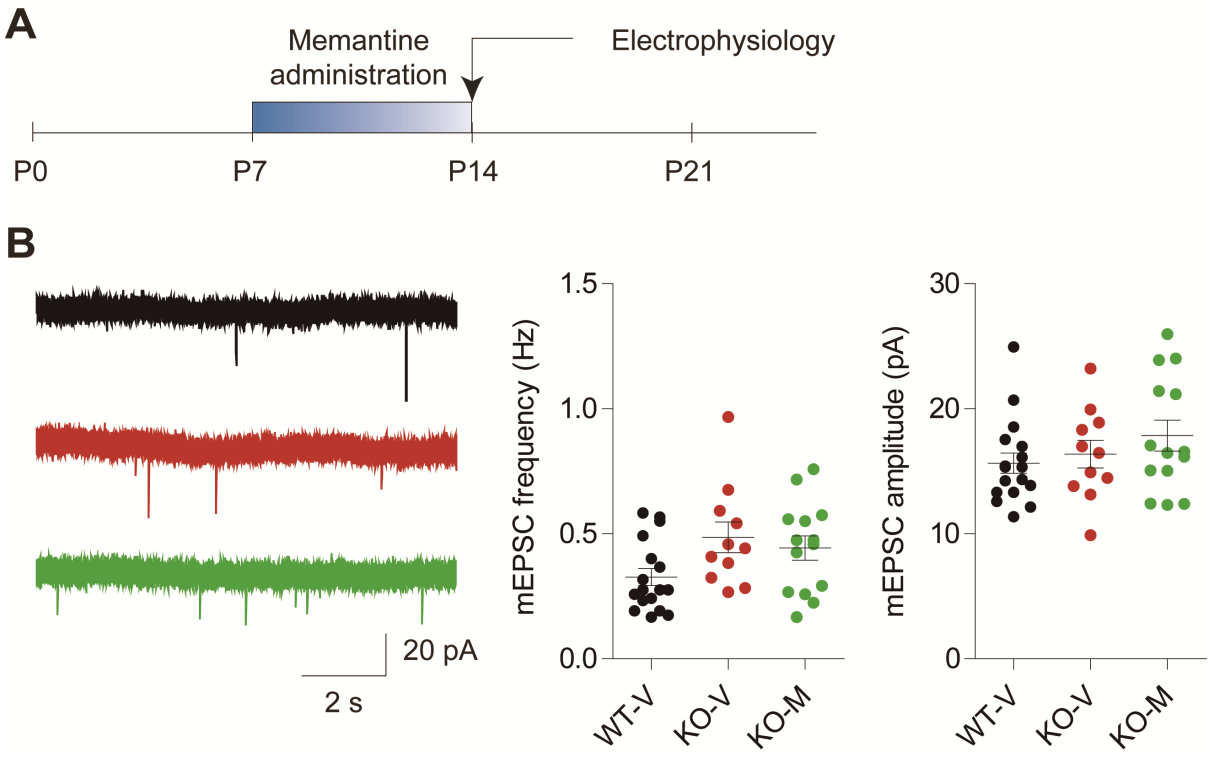

Figure S11. Early memantine treatment for a shorter period (P7–14) does not affect mEPSCs in the *Shank2*$^{-/-}$ hippocampus.

(A and B) Early memantine treatment for a shorter period (P7–14) has no effect on mEPSCs in *Shank2*$^{-/-}$ CA1 pyramidal neurons (P13–15 (n = 17 neurons from 3 mice for WT-V, 11 (2) for KO-V, and 14 (3) for KO-M, Kruskal-Wallis test).

Supplementary fig. 12

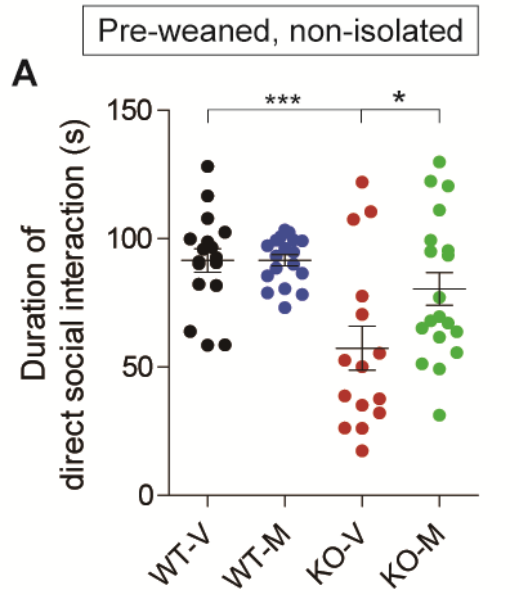

Figure S12. Early memantine treatment improves direct social interaction in juvenile *Shank2*$^{-/-}$ mice tested in the absence of isolation and before weaning.

(A) Early memantine treatment improves social interaction of juvenile *Shank2*$^{-/-}$ mice (P28–35) in the direct social interaction test, as indicated by time spent in social interaction. Young *Shank2*$^{-/-}$ mice were orally administered memantine (20 mg/kg) twice daily for 2 weeks from P7 to P21, followed by measurement of direct social interactions at juvenile (P28–35) stages in the absence of social isolation and weaning. (n = 17 mice (WT-V/vehicle), 18 (WT-M/memantine), 15 (KO-V), and 19 (KO-M), *P < 0.05, ***P < 0.001, ns, not significant, two-way ANOVA with Holm-Sidak test).

Supplementary fig. 13

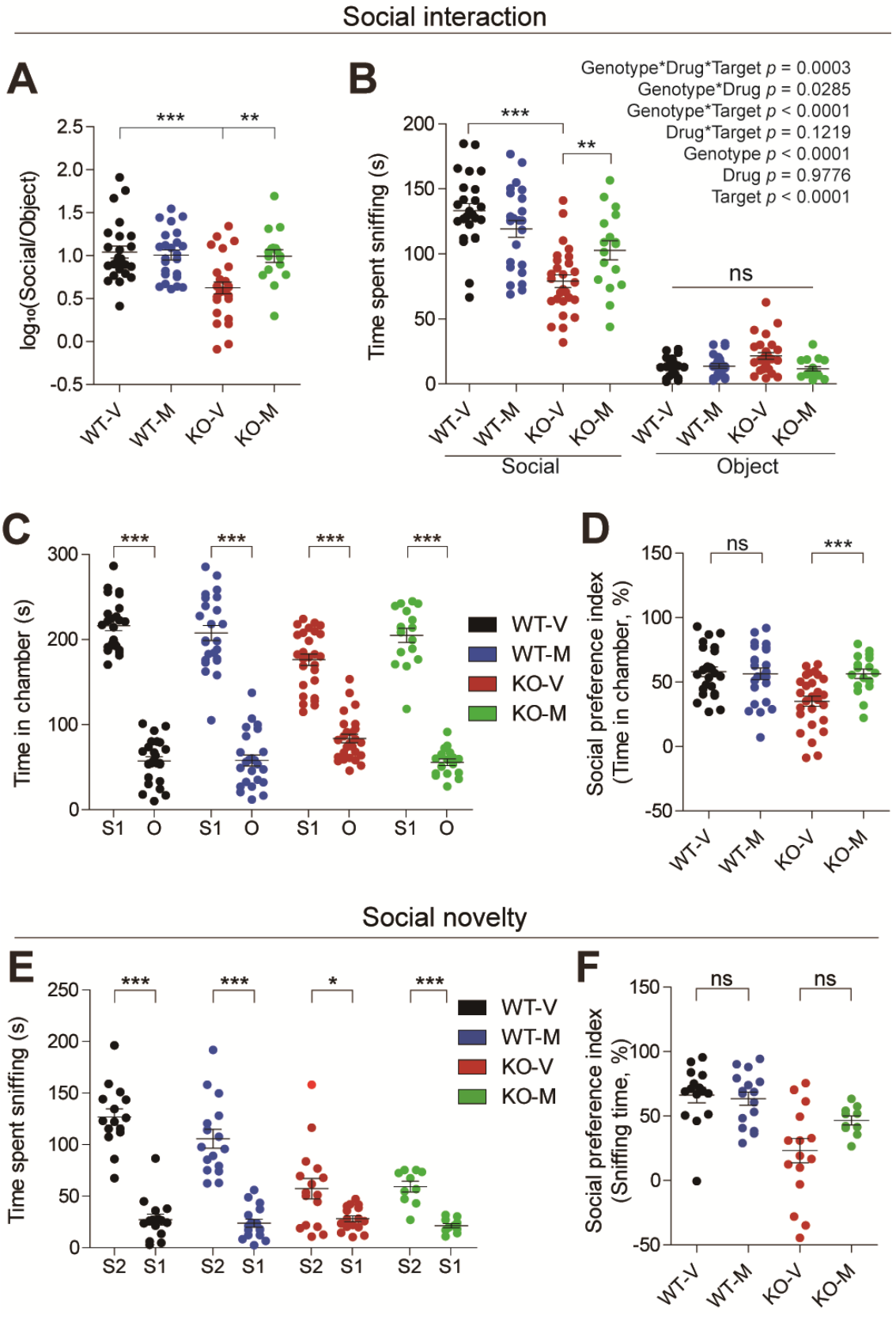

Figure S13. Early memantine treatment improves social approach but has no

effect on social novelty in adult *Shank2*$^{-/-}$ mice in the three-chamber test.

(A and B) Early memantine treatment improves social approach of adult *Shank2*$^{-/-}$ mice (>P56) in the three-chamber test, as shown by $\log_{10}$(Social/Object) values and time spent sniffing (S1/O). (n = 25 mice for WT-V, 24 for WT-M, 27 for KO-V, and 17 for KO-M, ***P* < 0.01, ****P* < 0.001, ns, not significant, two-way ANOVA with Holm-Sidak test for (A; there was a significant genotype x drug interaction) and three-way ANOVA with Bonferroni test for (B; main effect and interaction p values are indicated in the figure)). The $\log_{10}$(Social/Object) values were derived from the raw S1/O data to perform two-ANOVA analysis, based on the previous report that ratio values can be used for two-way ANOVA [17].

(C and D) Early memantine treatment improves social interaction of adult *Shank2*$^{-/-}$ mice (> P56) in the three-chamber social interaction test, as shown by time spent in chamber with S1/O (C; not time spent sniffing) and the social preference index (D). (n = 25 mice (WT-V), 24 (WT-M), 27 (KO-V), and 17 (KO-M), ****P* < 0.001, ns, not significant, paired Student's t-test (C), and unpaired Student's t-test for (D; two-way ANOVA was not performed because the social preference index is a normalized value)).

(E and F) Early memantine treatment (P7–21) has no effect on social novelty recognition of *Shank2*$^{-/-}$ mice (>P56) in the three-chamber test, as shown by the time spent sniffing S2/S1 (novel stranger/familiar stranger; E) and the social preference index based on sniffing time (F). (n = 15 mice for WT-V, 16 for WT-M, 16 for KO-V, and 10 for KO-M, **P* < 0.05, ****P* < 0.001, ns, not significant, paired Student's t-test or Wilcoxon matched pairs signed rank test for (E), and unpaired Student's test or Mann Whitney U test for (F).

Supplementary fig. 14

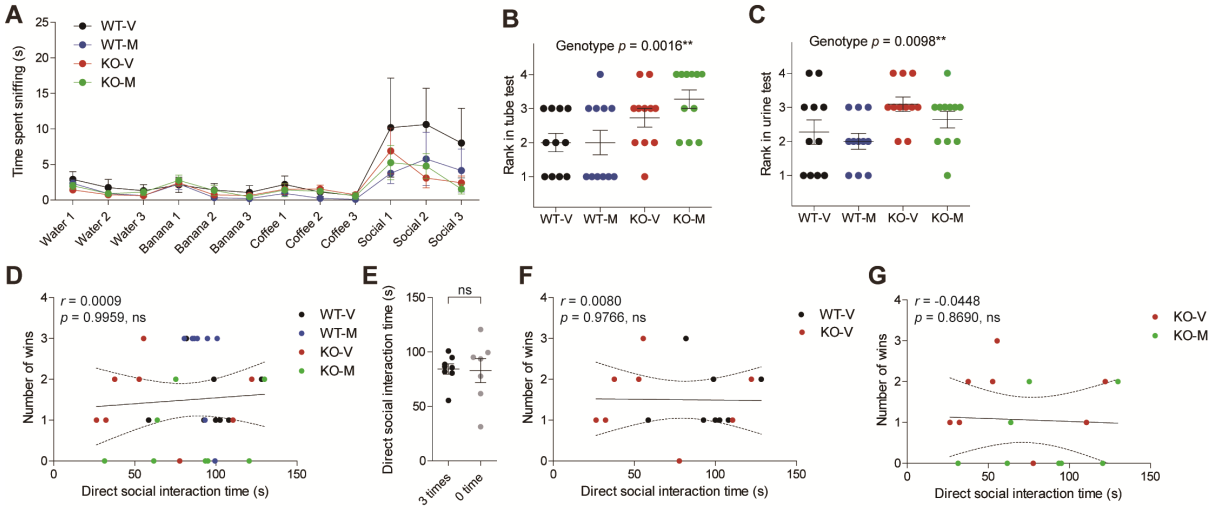

Figure S14. *Shank2*$^{-/-}$ mice display social submissiveness that is not associated with social interaction and is resistant to early memantine treatment in *Shank2*$^{-/-}$ mice.

(A) Early memantine treatment has no effect on olfactory function in *Shank2*$^{-/-}$ mice at P56. Young *Shank2*$^{-/-}$ mice were orally administered memantine (20 mg/kg) twice daily for 2 weeks during P7–21, followed by measurement of olfactory function during P56–70. (n = 20 mice for WT-V, 21 for WT-M, 21 for KO-V, and 22 for KO-M, ns, not significant, two-way ANOVA). Two-way ANOVA for each olfactory cues was performed for biologically better interpretations, which did not yield any significant genotype effect, drug effect, or genotype x drug interaction.

(B and C) *Shank2*$^{-/-}$ mice show submissiveness to WT mice in both tube and urine tests, as supported by the significant genotype effects. Note that early memantine treatment has no effect on social ranking in *Shank2*$^{-/-}$ mice at P56, as supported by the lack of main drug effects. Young *Shank2*$^{-/-}$ mice early memantine treated during P7–21 were subjected to two different social dominance tests during P56–90. (n = 11 mice for WT-V, WT-M, KO-V, and KO-M, $^{**}P < 0.01$, ns, not significant, two-way

ANOVA; post hoc comparisons were not performed due to the lack of significant genotype x drug interaction).

(D) Lack of correlation between social interaction (direct social interaction test) and number of wins (tube test) in WT and *Shank2*$^{-/-}$ mice. These mice represent a subset of the mice for which we presented the data in **Figure S12** and **Figure S14B-C**. This subset went through both direct social interaction and tube tests. Specifically, these mice were maintained under clear mixed genotype housing (MGH) starting from ~P7 after PCR genotyping and subjected to the direct social interaction test before weaning and without social isolation ~P28–33, followed by weaning, additional MGH for more than two weeks, and the tube test. The colored dots indicate individual mice in distinct experimental groups. (n = 8 mice for WT-V, 8 for WT-M, 8 for KO-V, and 8 for KO-M, Spearman's correlation).

(E) Lack of correlation between social interaction (direct social interaction test) and number of wins (tube test) in WT and *Shank2*$^{-/-}$ mice. Note that the mice who won three times in the tube test (highest ranking) and those who never won (lowest ranking) show comparable levels of direct social interaction. These mice were selected from the mice shown in (D). (n = 8 mice for 3 times and 7 for 0 time, ns, not significant, Mann-Whitney U test).

(F and G) Lack of correlation between social interaction (direct social interaction test) and number of wins (tube test) in sub-group comparison of W-V and KO-V mice, or KO-V and KO-M mice, derived from the mice mentioned above (D). (n = 8 mice for WT-V, 8 for WT-M, 8 for KO-V, and 8 for KO-M, ns, not significant, Spearman's correlation).

Supplementary fig. 15

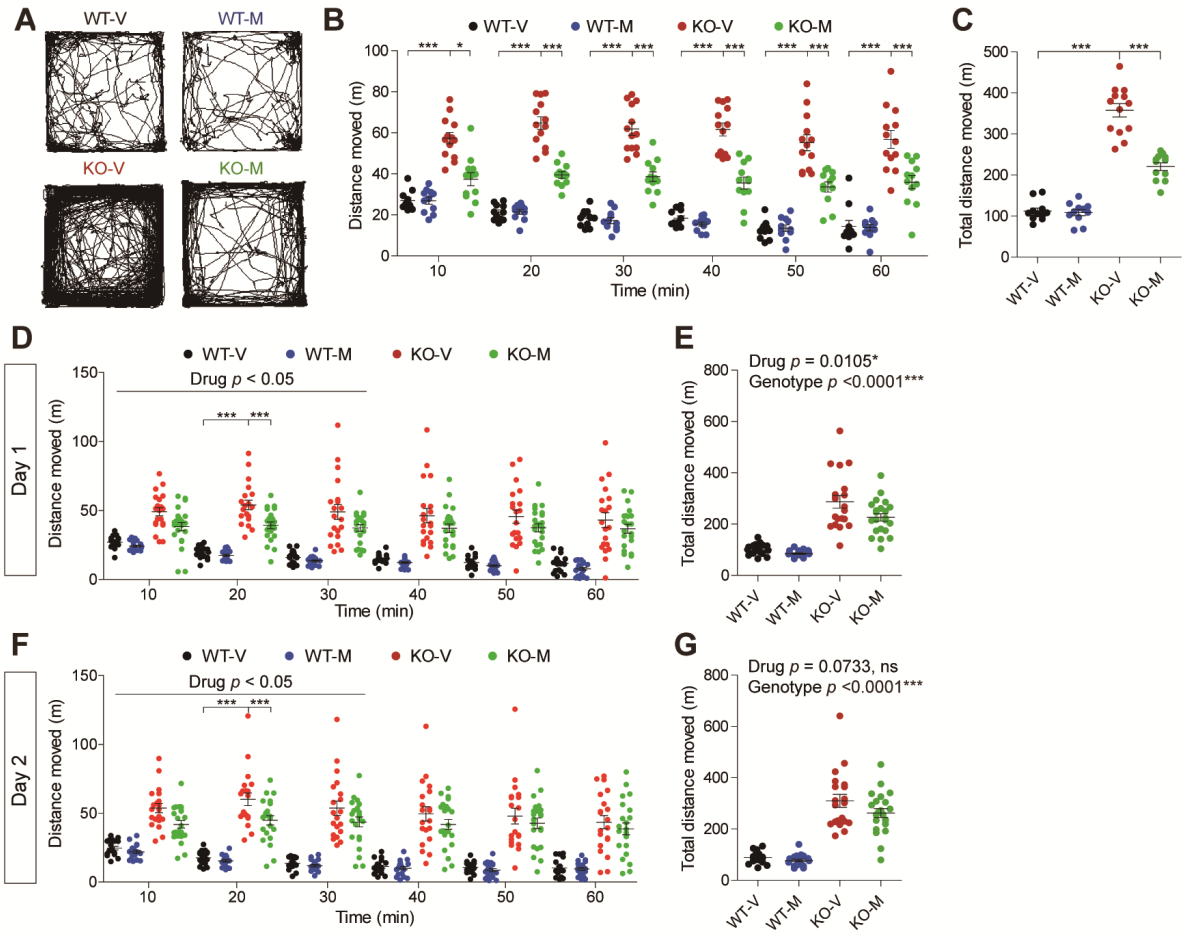

Figure S15. Early memantine treatment modestly improves hyperactivity in the open-field test in adult *Shank2*$^{-/-}$ mice, and habitation dampens the memantine-dependent improvement.

(A–C) Early memantine treatment partially improves hyperactivity of adult *Shank2*$^{-/-}$ mice (P56) in the open-field test (a novel environment). (n = 11 mice for WT-V, 11 for WT-M, 13 for KO-V, and 12 for KO-M, **P* < 0.05, ****P* < 0.001, ns, not significant, two-way ANOVA with Holm-Sidak (normal distribution) or Bonferroni (non-normal distribution) test for (B) and two-way ANOVA with Holm-Sidak test for (C)).

(D–G) Habituation dampens the effect of early memantine treatment on hyperactivity in adult *Shank2*$^{-/-}$ mice (P56) in an independent open-field test performed for two

consecutive days. *Shank2*$^{-/-}$ mice early memantine treated during P7–21 were subjected to open-field tests during P56–68 for two consecutive days. Note that the difference between memantine-treated and vehicle-treated *Shank2*$^{-/-}$ mice on day 2 became no longer significant, as compared with that on day 1 (E and G), suggestive of the influence of habituation. These results, which are not as strong as that from an independent experiment mentioned above (A–C), led to the collective conclusion that memantine moderately improves hyperactivity in *Shank2*$^{-/-}$ mice. (n = 19 mice for WT-V, 20 for WT-M, 20 for KO-V, and 22 for KO-M, **P* < 0.05, ****P* < 0.001, ns, not significant, two-way ANOVA with Holm-Sidak test (D; post hoc comparisons were only performed for the 10-min block that show significant genotype x drug interaction), two-way ANOVA for (e; genotype x drug interaction *P* > 0.05), two-way ANOVA with Bonferroni test (F), and two-way ANOVA for (G; genotype x drug interaction *P* > 0.05).

Supplementary fig. 16

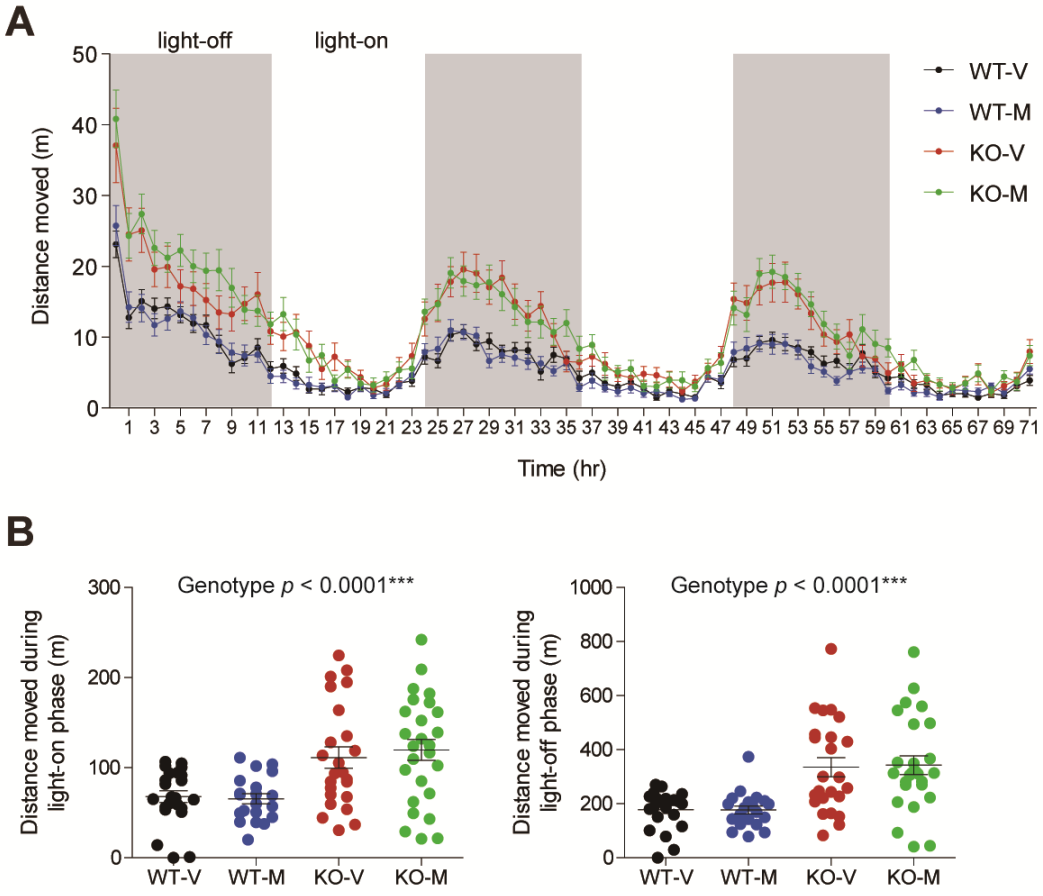

Figure S16. Early memantine treatment does not improve hyperactivity in adult *Shank2*$^{-/-}$ mice in the Laboras test (a familiar environment).

(A and B) Locomotor activity of *Shank2*$^{-/-}$ mice (2–3 months) early memantine treated during P7–21 were subjected to the Laboras test, where mouse movements in Laboras cages (a home cage-like environment) were measured for three consecutive days. Note that the locomotor activities of memantine-treated and vehicle-treated *Shank2*$^{-/-}$ mice on day 2 and 3 are comparable, suggesting that memantine has no effect on hyperactivity in a sufficiently familiar environment. Light-off phases are shown in shades. (n = 23 mice for WT-V, 20 for WT-M, 24 for KO-V, and 26 for KO-M, ***P < 0.001, two-way ANOVA for (B)). ANOVA was not performed for (A).

Supplementary fig. 17

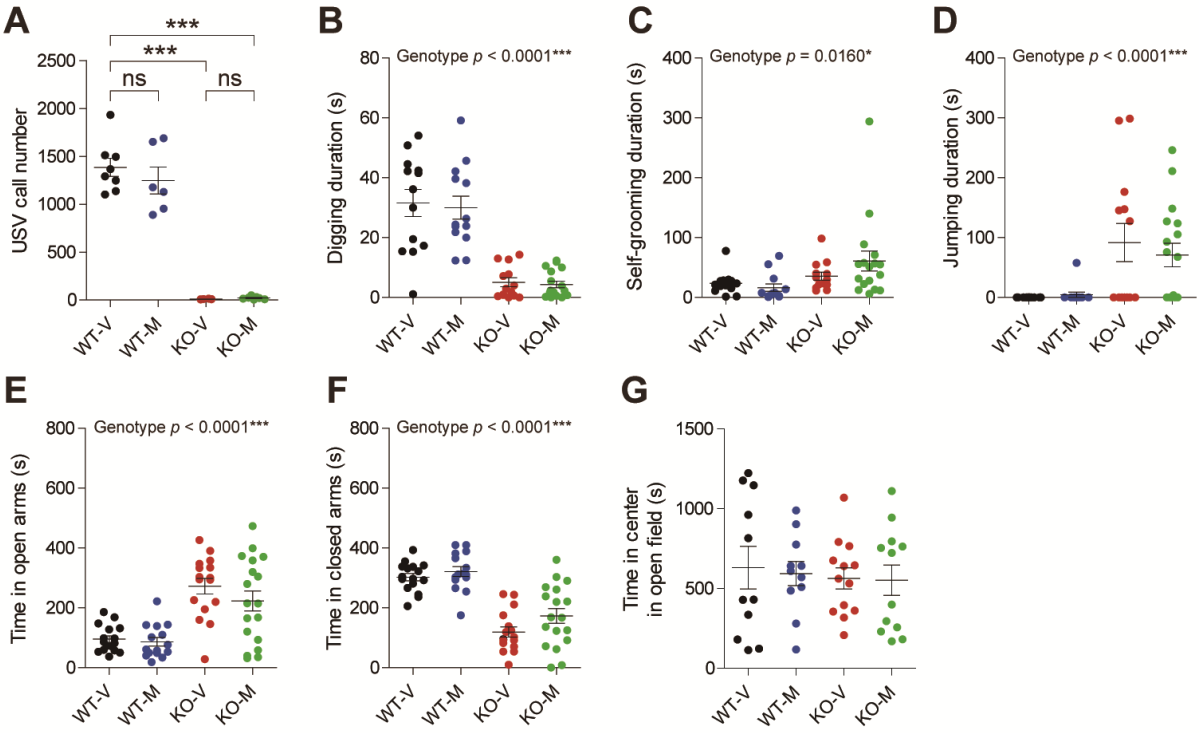

Figure S17. Early memantine treatment does not improve reduced USVs, enhanced repetitive behaviors, or enhanced anxiolytic-like behaviors in adult *Shank2*$^{-/-}$ mice.

(A) Number of USV calls in WT and *Shank2*$^{-/-}$ mice (> P56) treated early (P7–21) with memantine or vehicle. (n = 8 mice for WT-V, 6 for WT-M, 6 for KO-V, and 7 for KO-M, ***P < 0.001, ns, not significant, Mann Whitney U test or Student t-test).

(B–D) Repetitive behaviors (digging, self-grooming, and jumping) in memantine- and vehicle-treated (P7–21) WT and *Shank2*$^{-/-}$ mice (> P56). (n = 13 mice for WT-V, 13 for WT-M, 13 for KO-V, and 17 for KO-M, *P < 0.05, ***P < 0.001, two-way ANOVA).

(E and F) Elevated plus maze behaviors in memantine- and vehicle-treated (P7–21) WT and *Shank2*$^{-/-}$ mice (> P56). (n = 16 mice for WT-V, 15 for WT-M, 16 for KO-V, and 18 for KO-M, ***P < 0.001, two-way ANOVA).

(G) Time spent in the center region of the open-field arena in memantine- and vehicle-treated (P7–21) WT and *Shank2*$^{-/-}$ mice (> P56). (n = 11 mice for WT-V, 11 for WT-M, 13 for KO-V, and 12 for KO-M, two-way ANOVA).

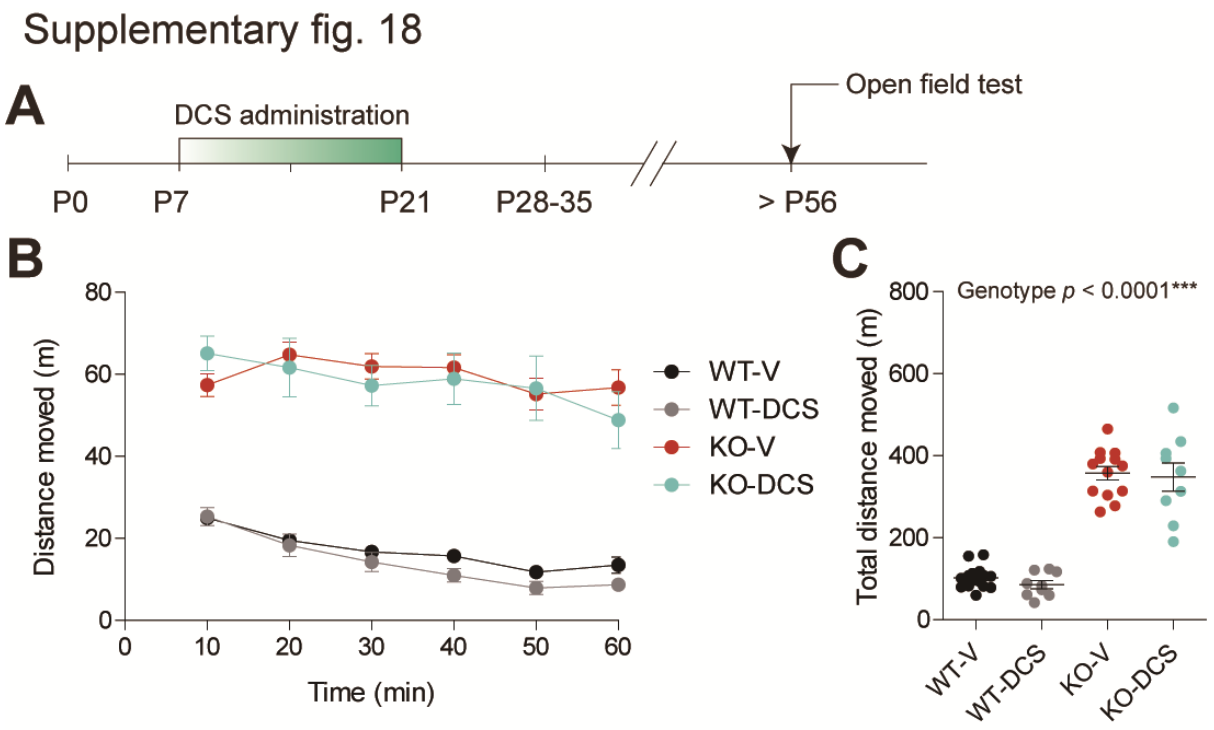

Figure S18. Early D-cycloserine treatment does not improve hyperactivity in adult *Shank2*$^{-/-}$ mice.

(A–C) Early D-cycloserine treatment fails to improve hyperactivity of adult *Shank2*$^{-/-}$ mice in the open-field test. (n = 16 mice (WT-V), 9 (WT-M), 13 (KO-V), and 9 (KO-M), ***P < 0.001, two-way ANOVA for (C)). ANOVA was not performed for (B).

Supplementary figure 19

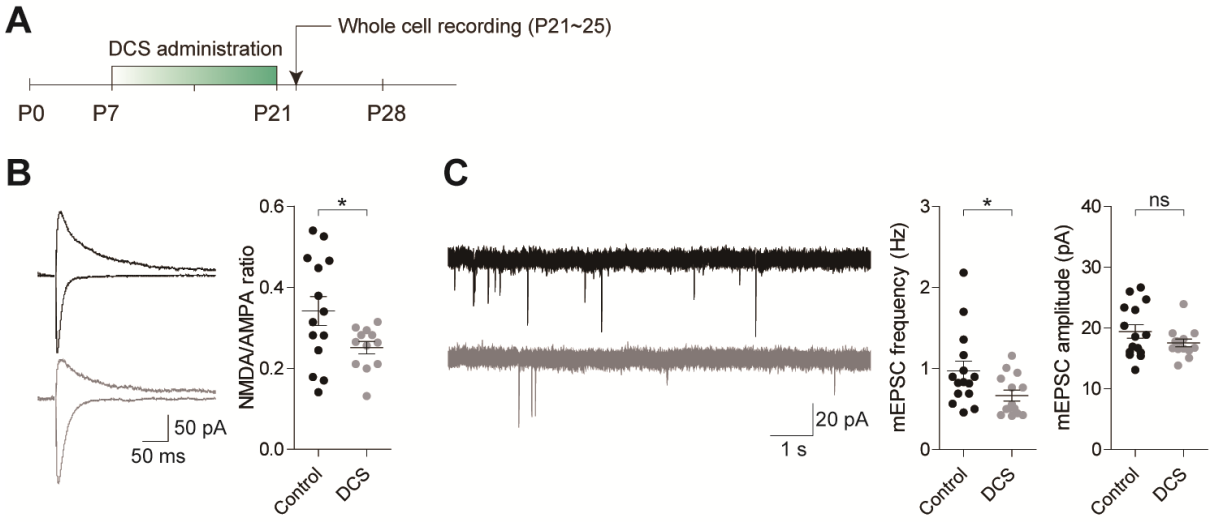

Figure S19. Early D-cycloserine treatment of WT mice during P7–21 suppresses NMDAR function at the juvenile stage.

(A and B) Early D-cycloserine treatment during P7–21 in WT mice (A) induces a decrease in the NMDA/AMPA ratio at the juvenile stage (~P21–25) (B). Young WT mice were orally administered D-cycloserine (40 mg/kg) twice daily for 2 weeks during P7–21 followed by measurements of the NMDA/AMPA ratio at SC-CA1 synapses at ~P21–25. (n = 14 neurons from 4 mice for control, 12 (5) for DCS, *$P < 0.05$, Student's t-test).

(C) Early D-cycloserine treatment during P7–21 in WT mice induces a decrease in mEPSC frequency but no effect on mEPSC amplitude at the juvenile stage (~P23–25). Young WT mice were orally administered D-cycloserine (40 mg/kg) twice daily for 2 weeks during P7–21 followed by measurements of mEPSCs in CA1 pyramidal neurons at ~P23–35. (n = 15 neurons from 3 mice for control, 14 (3) for DCS, *$P < 0.05$, ns, not significant, Mann Whitney U test).

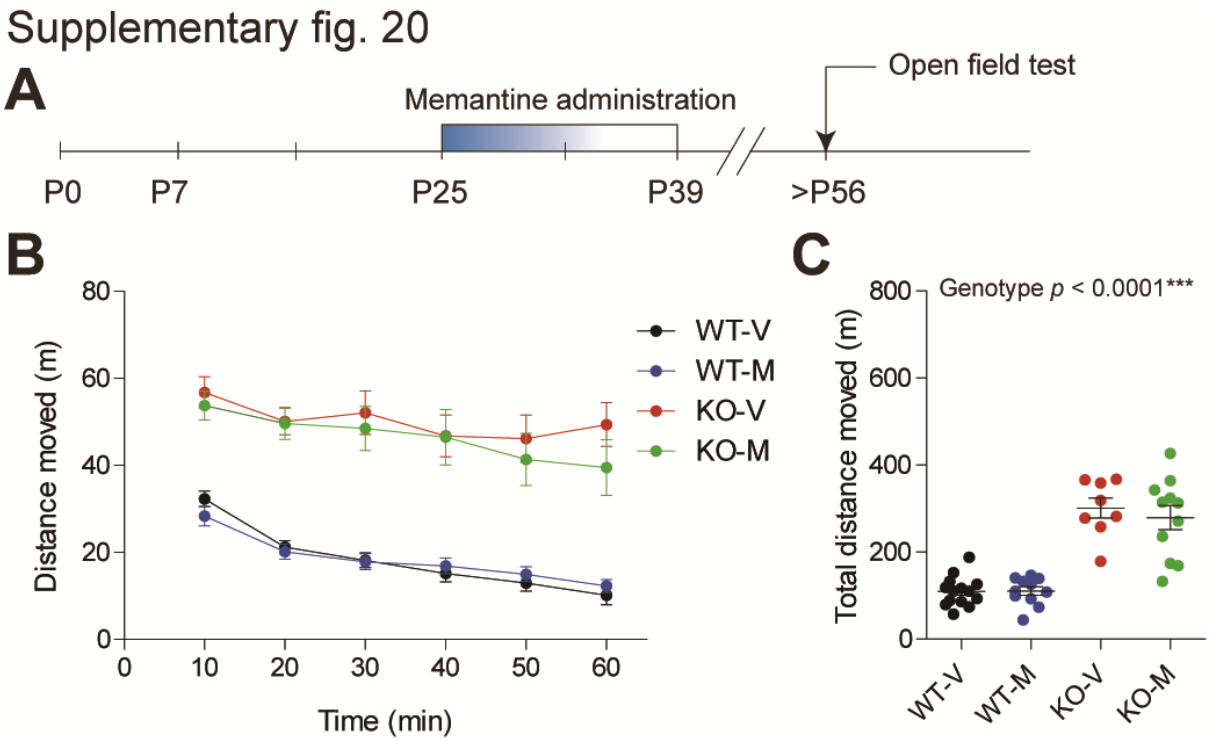

Figure S20. Late chronic memantine treatment does not improve hyperactivity in *Shank2*$^{-/-}$ mice.

(A–C) Late chronic memantine treatment fails to improve hyperactivity of adult *Shank2*$^{-/-}$ mice in the open-field test. (n = 14 mice for WT-V, 11 for WT-M, 8 for KO-V, and 11 for KO-M, ****P* < 0.001, two-way ANOVA for (C)). ANOVA was not performed for (B).

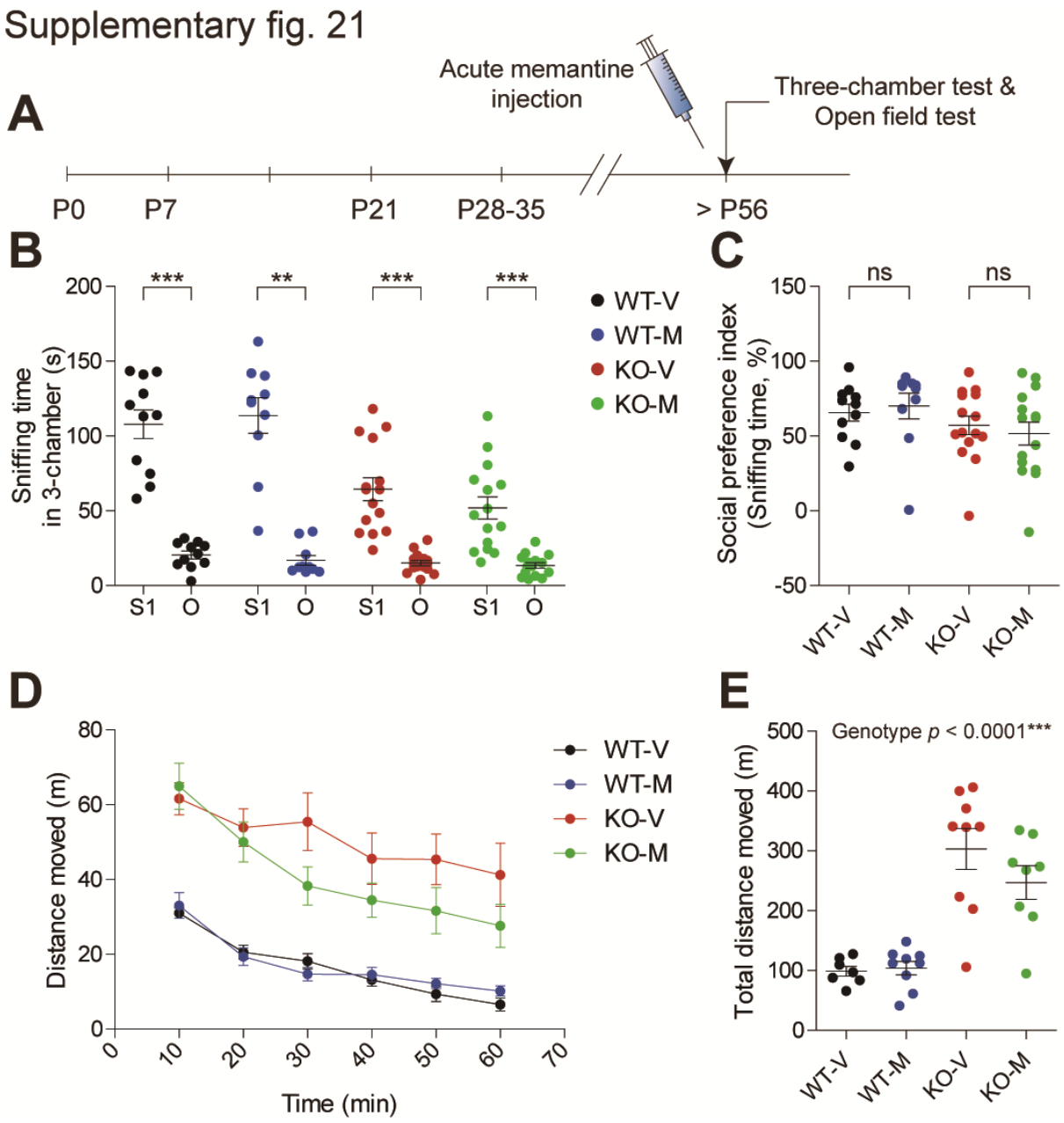

Figure S21. Late acute memantine treatment does not improve social interaction or hyperactivity in *Shank2*$^{-/-}$ mice.

(A) Schematic depiction of late acute memantine treatment. *Shank2*$^{-/-}$ mice were administered memantine acutely (10 mg/kg; intraperitoneal) at a later stage (~P56), followed by measurements of three-chamber social interaction and open-field hyperactivity 30 min after injection.

(B and C) Late acute memantine treatment fails to improve social interaction in

Shank2$^{-/-}$ mice in the three-chamber social interaction test, as indicated by time sniffing S1/O and the social preference index based on sniffing time. (n = 11 mice for WT-V, 10 for WT-M, 15 for KO-V, and 15 for KO-M, ***P* < 0.01, ****P* < 0.001, ns, not significant, paired Student's t-test or Wilcoxon matched pairs signed rank test for (B), and unpaired Student's t-test or Mann Whitney U test for (C; two-way ANOVA was not performed because the social preference index is a normalized value)).

(D and E) Late acute memantine treatment fails to improve hyperactivity of adult *Shank2*$^{-/-}$ mice in the open-field test. (n = 7 mice (WT-V), 9 (WT-M), 9 (KO-V), and 8 (KO-M), ****P* < 0.001, two-way ANOVA for (D)). ANOVA was not performed for (E).

Supplementary fig. 22

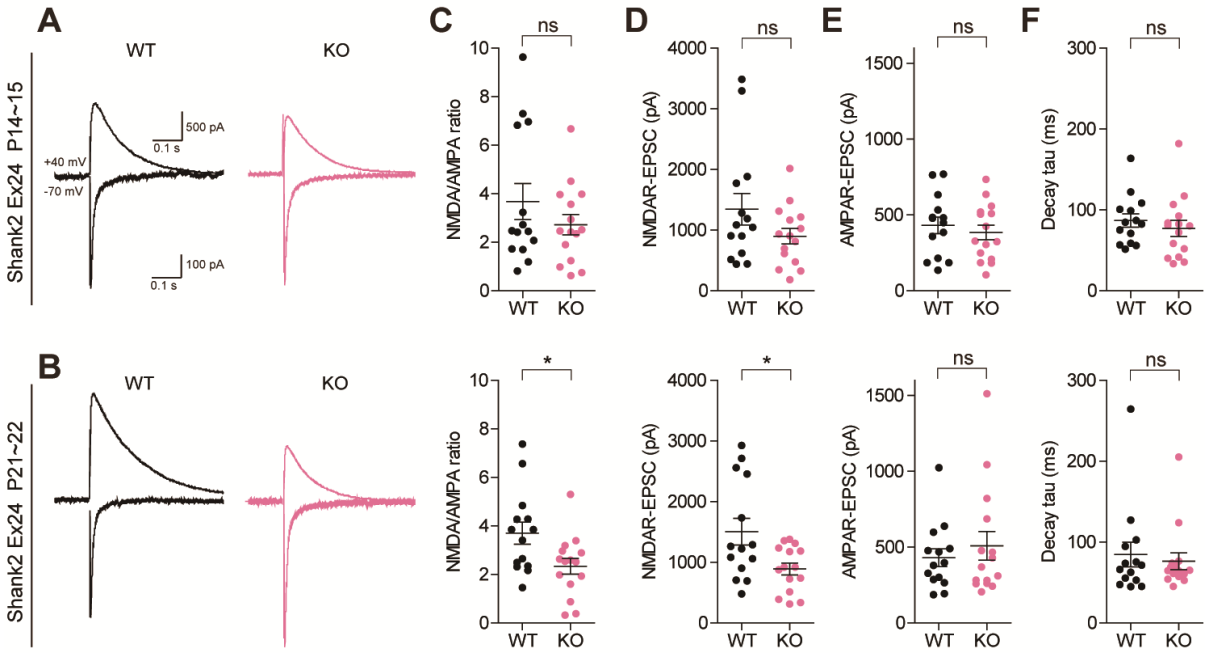

Figure S22. *Shank2*$^{-/-}$ mice lacking exon 24 show suppressed NMDAR function at ~P21 but normal NMDAR function at ~P14.

(A and B) Example traces of evoked NMDAR-EPSCs (at +40 mV) and AMPAR-EPSCs (at -70 mV) at *Shank2*$^{-/-}$ hippocampal SC-CA1 synapses at P14–15 (A) and P21–22 (B). Represented traces were obtained from WT (black) and *Shank2*$^{-/-}$ (red) mice. Both NMDAR- and AMPAR-mediated currents were elicited by 0.25 ms duration and 300 mA stimulation intensity in the same cell. Evoked AMPAR-EPSC recordings were carried out in the presence of the $GABA_A$ receptor antagonist picrotoxin (60 mM) at the holding potential of -70 mV; then NMDAR-EPSC recordings were followed by DNQX (20 mM) treatment and with the same stimulation pulse at the holding potential of +40 mV.

(C) NMDA/AMPA ratio at WT and *Shank2*$^{-/-}$ SC-CA1 synapses at P14–15 and P21–22. (P14–15, n = 14 neurons from 3 mice for WT and 15 (3) for KO; P21–22, n = 14 (3) for WT and 15 (3) for KO; *P < 0.05 [p = 0.0204], ns, not significant [p = 0.2643],

unpaired Student t-test).

(D) NMDAR-mediated EPSCs at WT and *Shank2*$^{-/-}$ SC-CA1 synapses at P14–15 and P21–22. (P14–15, n = 14 neurons from 3 mice for WT and 15 (3) for KO; P21–22, n = 14 (3) for WT and 15 (3) for KO; **P* < 0.05 [p = 0. 0146], ns, not significant [p = 0.1265], unpaired Student t-test).

(E) AMPAR-mediated EPSCs at WT and *Shank2*$^{-/-}$ SC-CA1 synapses at P14–15 and P21–22. (P14–15, n = 14 cells from 3 mice for WT and 15 (3) for KO; P21–22, n = 14 (3) for WT and 15 (3) for KO; ns, not significant [p = 0.5100 for 14–15 and 0.4932 for P21–22], unpaired Student t-test).

(F) Decay kinetics of NMDAR-mediated EPSCs at WT and *Shank2*$^{-/-}$ SC-CA1 synapses at P14–15 and P21–22. (P14–15, n = 14 neurons from 3 mice for WT and 15 (3) for KO; P21–22, n = 14 (3) for WT and 15 (3) for KO; ns, not significant [p = 0.4640 for 14–15 and 0.6517 for P21–22], unpaired Student t-test).

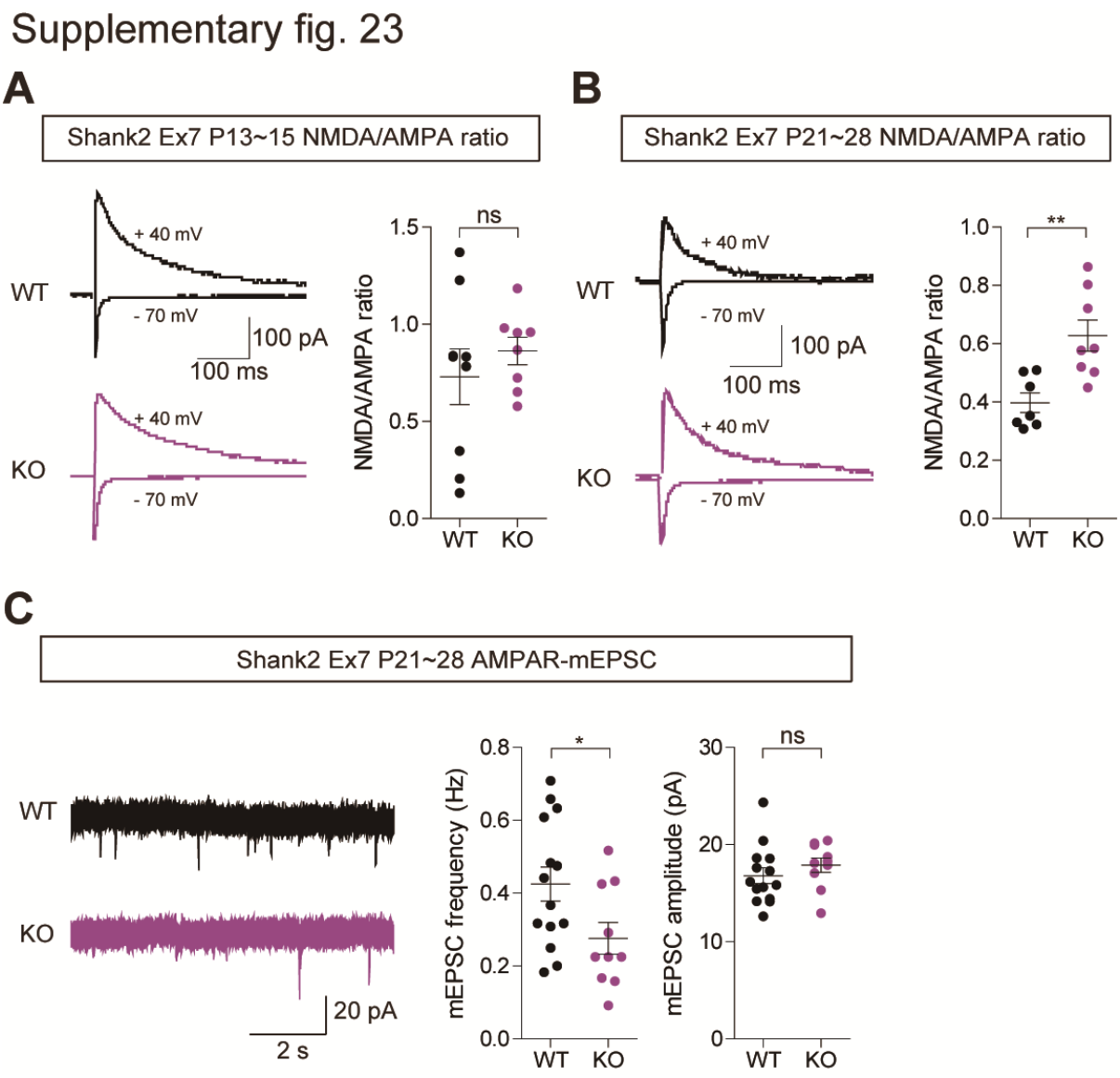

Figure S23. *Shank2*$^{-/-}$ mice lacking exon 7 show enhanced NMDAR function at ~P24 but normal NMDAR function at ~P14.

(A) Normal NMDA/AMPA ratio at *Shank2*$^{-/-}$ SC-CA1 synapses at P13–15. (n = 9 neurons from 3 mice for WT and 8 neurons from 3 mice for KO, ns, not significant, Student t-test).

(B) Increased NMDA/AMPA ratio at *Shank2*$^{-/-}$ SC-CA1 synapses at P21–28. (n = 7 neurons from 3 mice for WT and 8 neurons from 3 mice for KO, $^{**}P < 0.01$, Student t-test).

(C) Normal mEPSCs in *Shank2*$^{-/-}$ CA1 pyramidal neurons at P21–28. (n = 14 neurons from 4 mice for WT and 10 (4) for KO; **P* < 0.05, ns, not significant, Student t-test).

Supplementary fig. 24

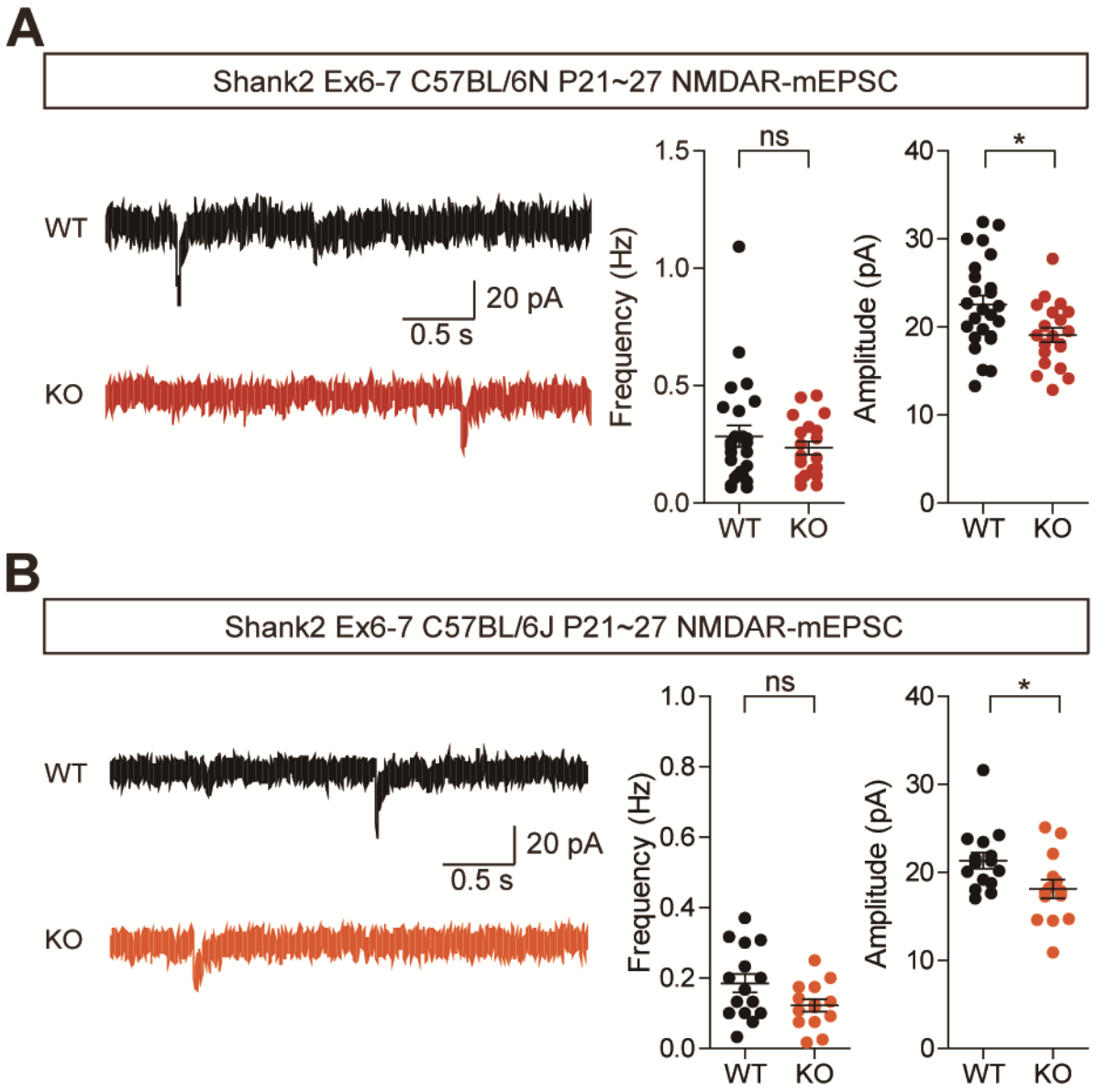

Figure S24. Similarly reduced amplitudes of NMDAR-mEPSCs in two *Shank2*$^{-/-}$ mouse lines in different genetic backgrounds (C57BL/6N and C57BL/6J).

(A and B) Reduced amplitude but normal frequency of NMDAR-mediated mEPSCs in *Shank2*$^{-/-}$ CA1 pyramidal neurons from mice in two different genetic backgrounds (C57BL/6N and C57BL/6J) at P21–27. We attempted the new genetic background (C57BL/6J) because the two backgrounds have previously been shown to affect various mouse phenotypes, including synaptic properties, caused by a point mutation

in the *Cyfip2* gene [18]. (C57BL/6N, n = 25 neurons from 4 mice for WT and 20 (4) for KO; C57BL/6J, n = 15 (3) for WT and 14 (5) for KO; *$P < 0.05$, ns, not significant, Mann-Whitney U test for (6N-frequency and 6J-amplitude) and Student t-test for (6N-amplitude and 6J-frequency)).

Supplementary fig. 25

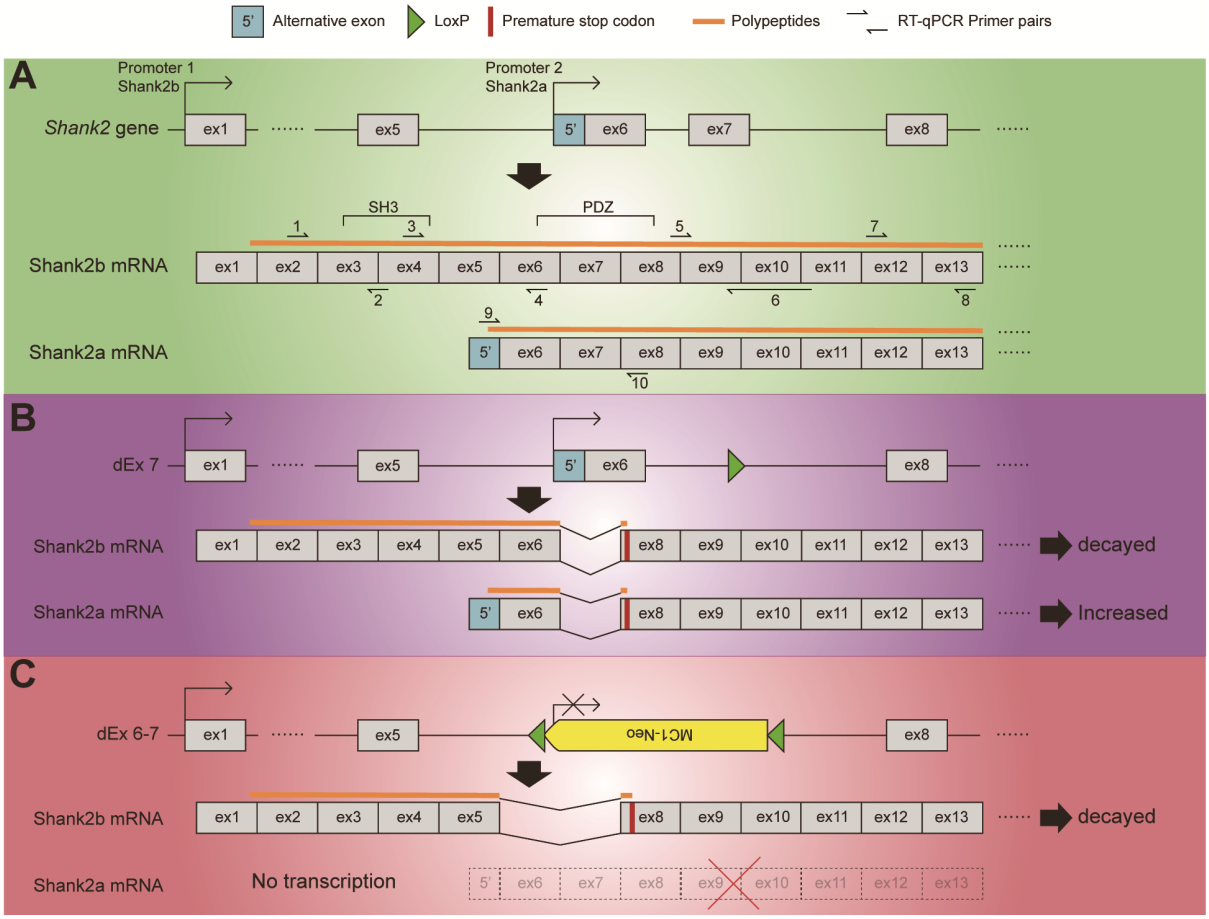

Figure S25. Schematic depiction of differential splice variants of Shank2 in *Shank2*$^{-/-}$ mice lacking exon 6–7 and exon 7.

(A) Schematic depiction of the structure of the *Shank2* gene and its two splice variants (short Shank2a and long Shank2b). Note that the short Shank2a splice variant is generated by alternative transcriptional initiation starting from a less known Shank2a-specific exon (termed here exon 5') located between exons 5 and 6 in the *Shank2* gene. The target locations of the primers used for RT-qPCR reactions are indicated.

(B) Schematic of the Shank2b and Shank2a splice variants in *Shank2*$^{-/-}$ mice lacking exon 7 (termed *Shank2*-dEx7 mice). Note that near full-length Shank2b and Shank2a splice variants lacking the exon 7 region are produced by transcription, which are decayed by ~75% and markedly increased in amounts, respectively (see the specific

RT-qPCR results in **Figure S26**). Note that the exon 7 deletion may lead to a premature protein truncation in both Shank2a and Shank2b proteins, and a marked increase in the levels of a short peptide (57 aa-long) derived from Shank2a.

(C) Schematic of the Shank2b and Shank2a splice variants in *Shank2*$^{-/-}$ mice lacking exons 6–7 (termed *Shank2*-dEx6–7 mice). Note that a near full-length Shank2b splice variant lacking exons 6–7 is produced, similar to the case of exon 7 deletion, whereas the Shank2a splice variant is not produced at all because the exon 5' (the first exon in the Shank2a transcript) is deleted together with exons 6 and 7 during homologous recombination by the gene-targeting construct (see the RT-qPCR results below).

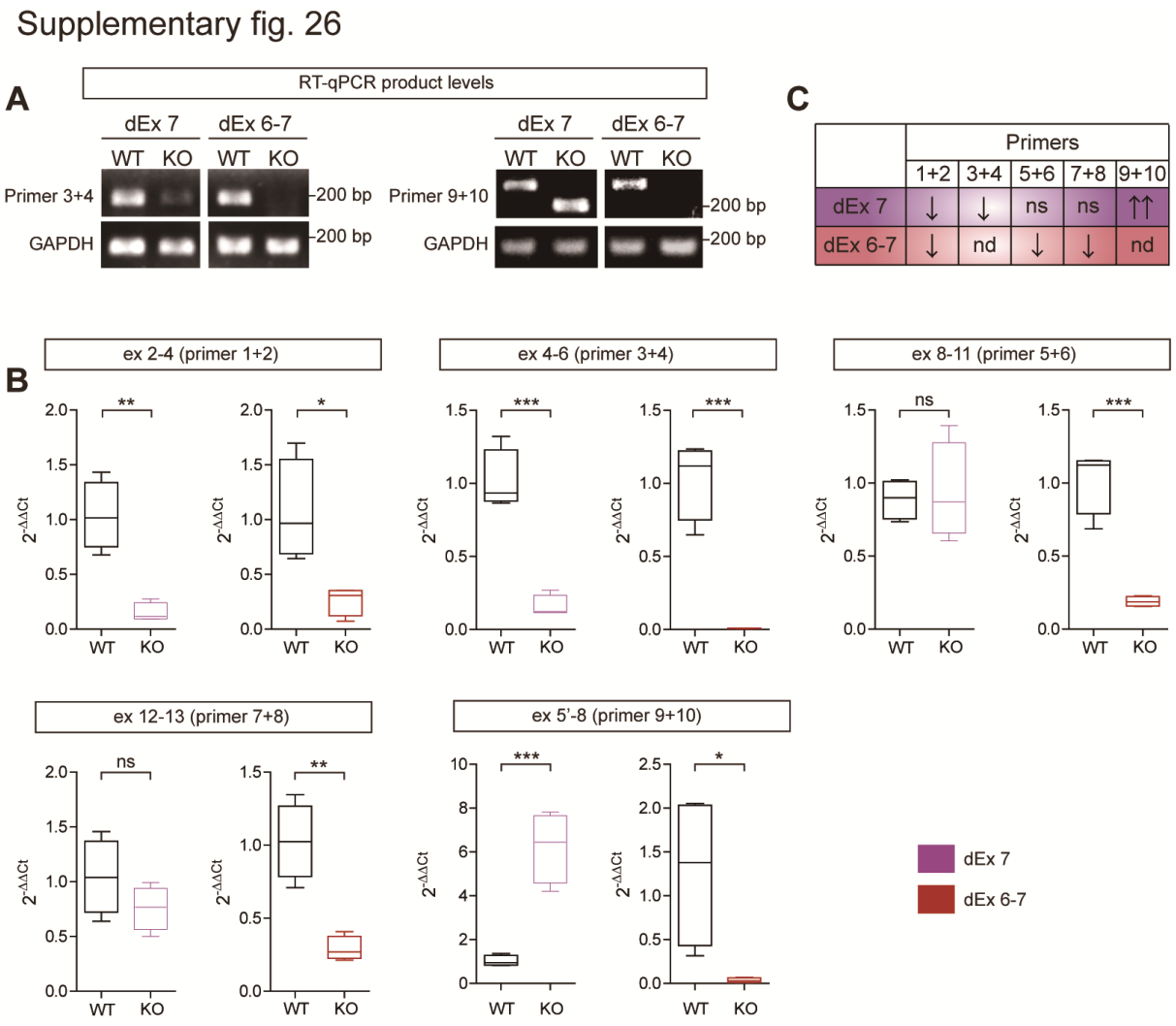

Figure S26. RT-qPCR results supporting differential splice variants of Shank2 in *Shank2*$^{-/-}$ mice lacking exon 6–7 and exon 7.

(A) Examples of the results of RT-qPCR performed using hippocampal samples from *Shank2*-dEx7 and *Shank2*-dEx6–7 mice (P25–28) and primers 3 + 4 and 9 + 10. Note that the levels of RT-qPCR products amplified using primers 3 + 4 are decreased (~25% of WT levels) in *Shank2*-dEx7 mice but almost completely disappeared in *Shank2*-dEx6–7 mice (see also the quantification of the results in panel B), indicative of the decay of the Shank2b variant in *Shank2*-dEx7 mice and support the lack of exon 6 in the Shank2b variant in *Shank2*-dEx6–7 mice. In contrast, RT-qPCR products from primers 9 + 10 are strongly increased in *Shank2*-dEx7 mice (~6-fold; see also the

quantification in panel B), whereas they are markedly decreased in *Shank2*-dEx6–7 mice caused by the loss of the first exon (exon 5'), suggesting that there is a marked difference in the levels of the Shank2a splice variant in the two mouse lines.

(B and C) Quantification (B) and summary (C) of the results of RT-qPCRs performed using hippocampal samples from *Shank2*-dEx7 and *Shank2*-dEx6–7 mice (P25–28) and various combinations of primers indicated in **Figure S25**. The results of RT-qPCRs using additional primer combinations can be interpreted in the following ways: the results with primers 3 + 4 indicate the decay of the Shank2b variant in *Shank2*-dEx7 mice and support the lack of exon 6 in the Shank2b variant in *Shank2*-dEx6–7 mice; the results with primers 5 + 6, or 7 + 8, indicate the decay of the Shank2b variant as well as a large abnormal increase of the Shank2a variant in *Shank2*-dEx7 mice, as mentioned above, and support the decay of the Shank2b variant in *Shank2*-dEx6–7 mice. (n = 4 mice for WT and KO, **P* < 0.05, ***P* < 0.01, ****P* < 0.001, ns, not significant, nd, not detected, Student t-test).

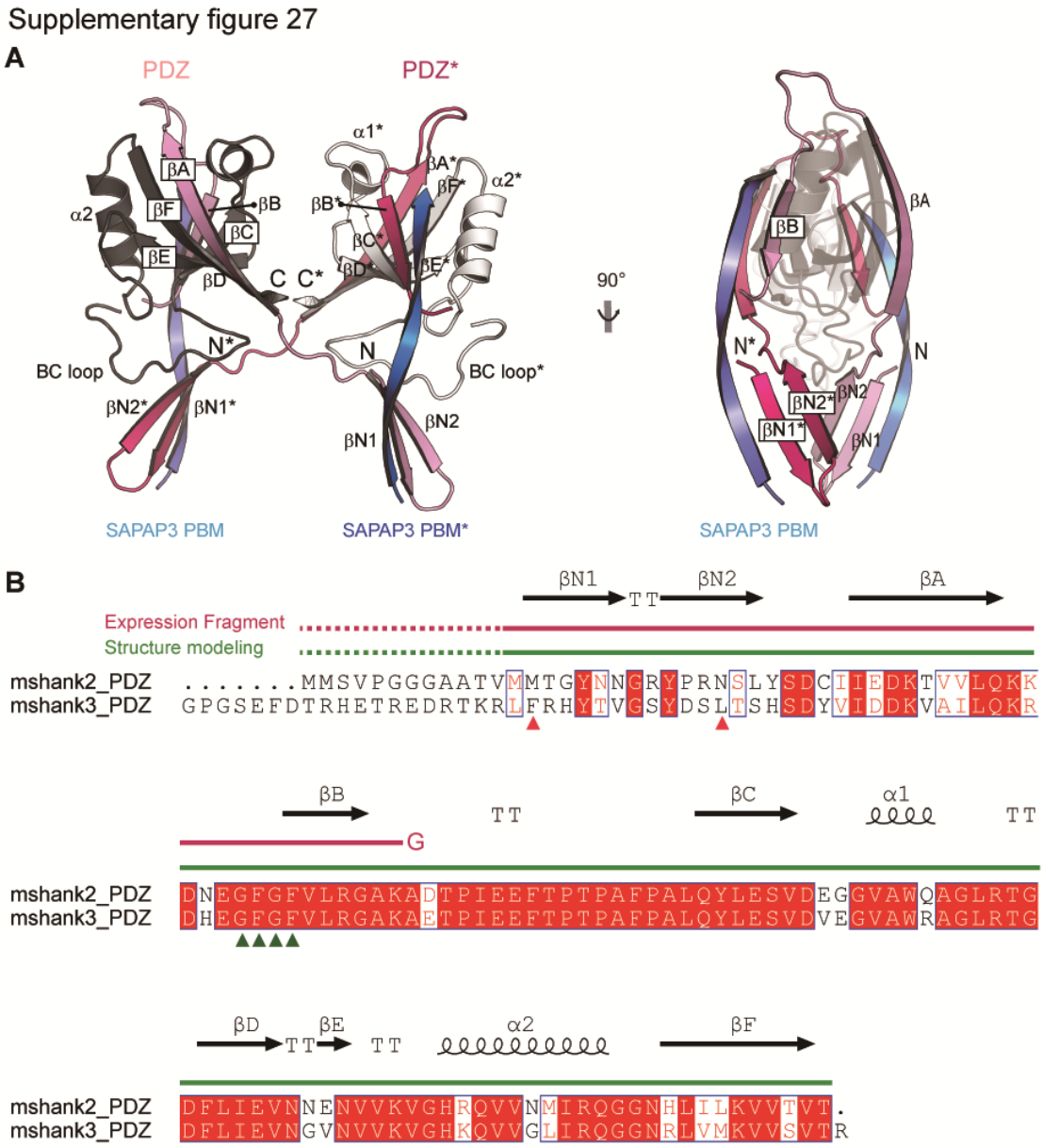

Figure S27. Molecular modeling of the Shank2 PDZ domain in complex with the C-terminal tail of SAPAP3 suggests that the short truncated peptide derived from the Shank2a splice variant in *Shank2*-dEx7 mice may compete with the full-length Shank2 PDZ domain for SAPAP3 binding.

(A and B) Molecular modeling of the mouse Shank2 PDZ domain in complex with the C-terminal PDZ-binding motif of SAPAP3 (A) and an alignment of the amino acid (aa) sequences of mouse Shank3 and Shank2 sequences in the PDZ domains and the aa

stretches in the immediate upstream regions (termed N-PDZ or N-terminal extended PDZ) (B), which (those of Shank3) have been shown to form a tight complex with the extended C-terminal PDZ-binding motif (E-PBM) of SAPAP3 [14]. Note that the E-PBM of SAPAP (blue) binds to three prominent sub-structures in the N-PDZ domain of Shank2 (pink), including the bN1 and bN2 strands in the N-terminal extended region, the BC loop located between bB and bC, and the PBM-binding pocket formed by bA*, bB*, and a2*. Note also that the short truncated peptide of Shank2a mimicking the N-terminal part of the N-PDZ domain of the mouse Shank2 might compete with the full-length N-PDZ domain of Shank2 for SAPAP3-PBM binding. Asterisks denote second molecules in the domain swapped dimer model. In the sequence alignment of Shank2/3 PDZ domains, identical and similar residues indicated by red filled boxes and red letters in open boxes, respectively. The secondary structures corresponding to a-helix, b-sheet, and b turns are indicated by squiggles, black arrows, and TT, respectively. The residues in the PDZ domain involved in the formation and binding for the C-terminal carboxylate of SAPAP3 (X1-F1-G-F2, X: any amino acids; F: hydrophobic residues; G: Gly) and the second hydrophobic pocket in the PDZ domain are indicated by green and red triangles, respectively. The magenta and green solid lines above the aa sequences indicates the short truncated peptide derived from Shank2a in Shank2-dEx7 mice and the full-length Shank2a PDZ domain, respectively. The dotted lines indicate unmodeled regions due to the lack of sufficient similarity for homology modeling. The indicated secondary structures and aa sequence alignment were acquired using the web-based software ESPript version 3.0 [19].

Supplementary Tables *(see separate Excel files)*

Table S1. All RNA-Seq data from WT and *Shank2*$^{-/-}$ mice at P14 and P25.

Table S2. (A) DEGs from naïve P14 KO (*Shank2*$^{-/-}$) and WT mice. (B) Summary of normalized read counts of DEGs for P14. (C) DEGs from naïve P25 KO and WT mice. (D) Summary of normalized read counts of DEGs for P25. (E) Summary of RNA-Seq mapping results from naïve P14 and P25 *Shank2*$^{-/-}$ and WT mice.

Table S3. GSEA using KO/WT query gene lists at P14 and P25 and C2 target gene sets.

Table S4. GSEA using KO/WT query gene lists at P14 and P25 and C5 target gene sets.

Table S5. Summary of electrophysiological results from *Shank2*$^{-/-}$ mice lacking exon 6–7.

Table S6. Statistical results.

Supplementary References

1. Silverman, J.L., Yang, M., Lord, C. & Crawley, J.N. Behavioural phenotyping assays for mouse models of autism. *Nature reviews. Neuroscience* 11, 490-502 (2010).

2. Yang, M., Silverman, J.L. & Crawley, J.N. Automated three-chambered social approach task for mice. *Current protocols in neuroscience / editorial board, Jacqueline N. Crawley ... [et al.]* Chapter 8, Unit 8 26 (2011).

3. Won, H.*, et al.* Autistic-like social behaviour in Shank2-mutant mice improved by restoring NMDA receptor function. *Nature* 486, 261-265 (2012).

4. Bolivar, V.J., Walters, S.R. & Phoenix, J.L. Assessing autism-like behavior in mice: variations in social interactions among inbred strains. *Behavioural brain research* 176, 21-26 (2007).

5. McFarlane, H.G.*, et al.* Autism-like behavioral phenotypes in BTBR T+tf/J mice. *Genes, brain, and behavior* 7, 152-163 (2008).

6. Yang, M. & Crawley, J.N. Simple behavioral assessment of mouse olfaction. *Current protocols in neuroscience / editorial board, Jacqueline N. Crawley ... [et al.]* Chapter 8, Unit 8 24 (2009).

7. Wang, F.*, et al.* Bidirectional control of social hierarchy by synaptic efficacy in medial prefrontal cortex. *Science* 334, 693-697 (2011).

8. Attwell, D. & Gibb, A. Neuroenergetics and the kinetic design of excitatory synapses. *Nature reviews. Neuroscience* 6, 841-849 (2005).

9. Kim, M.H.*, et al.* Enhanced NMDA receptor-mediated synaptic transmission, enhanced long-term potentiation, and impaired learning and memory in mice lacking IRSp53. *The Journal of neuroscience : the official journal of the Society for Neuroscience* 29, 1586-1595 (2009).

10. Kim, D., Langmead, B. & Salzberg, S.L. HISAT: a fast spliced aligner with low memory requirements. *Nature methods* 12, 357-360 (2015).

11. Anders, S., Pyl, P.T. & Huber, W. HTSeq--a Python framework to work with high-throughput sequencing data. *Bioinformatics* 31, 166-169 (2015).

12. Love, M.I., Huber, W. & Anders, S. Moderated estimation of fold change and dispersion for RNA-seq data with DESeq2. *Genome biology* 15, 550 (2014).

13. Subramanian, A.*, et al.* Gene set enrichment analysis: a knowledge-based approach for interpreting genome-wide expression profiles. *Proceedings of the National Academy of Sciences of the United States of America* 102, 15545-15550 (2005).

14. Zeng, M.*, et al.* A binding site outside the canonical PDZ domain determines the specific interaction between Shank and SAPAP and their function.

Proceedings of the National Academy of Sciences of the United States of America 113, E3081-3090 (2016).

15. Biasini, M.*, et al.* SWISS-MODEL: modelling protein tertiary and quaternary structure using evolutionary information. *Nucleic Acids Res* 42, W252-258 (2014).

16. DeLano, W.L. PyMOL molecular viewer: Updates and refinements. *Abstr Pap Am Chem S* 238(2009).

17. Anderson, D.E. & Lydic, R. On the effect of using ratios in the analysis of variance. *Biobehav Rev* 1, 225-229 (1977).

18. Kumar, V.*, et al.* C57BL/6N mutation in cytoplasmic FMRP interacting protein 2 regulates cocaine response. *Science* 342, 1508-1512 (2013).

19. Robert, X. & Gouet, P. Deciphering key features in protein structures with the new ENDscript server. *Nucleic Acids Res* 42, W320-324 (2014).